# Momentum space approach to microscopic effects in elastic proton scattering

A. Picklesimer
*Department of Physics and Astronomy, University of Maryland, College Park, Maryland 20742*
*and Los Alamos National Laboratory, Los Alamos, New Mexico 87545*

P. C. Tandy
*Department of Physics, Kent State University, Kent, Ohio 44242*
*and Los Alamos National Laboratory, Los Alamos, New Mexico 87545*

R. M. Thaler
*Department of Physics, Case Western Reserve University, Cleveland, Ohio 44106*
*and Los Alamos National Laboratory, Los Alamos, New Mexico 87545*

D. H. Wolfe
*Department of Physics, Kent State University, Kent, Ohio 44242*
(Received 6 August 1984)

The microscopic nonrelativistic first-order optical potential for proton-nucleus scattering is studied in some detail. Momentum-space calculations have been performed for a number of different target nuclei at proton energies above $\sim 100$ MeV and these microscopic predictions are compared with experimental cross section, analyzing power, and spin-rotation function data. The input to these calculations consists of the free on-shell nucleon-nucleon $t$ matrix, its nonlocal and off-shell structure, the treatment of the full-folding integral, and target densities obtained from electron scattering. Off-shell and nonlocal effects, as well as various factorization approximations, are studied. The sensitivity to uncertainties in the off-shell extension of the $t$ matrix, within the context of the Love-Franey model, is explicitly displayed. Similarly, uncertainties due to nonlocalities and incomplete knowledge of nuclear densities are shown. Explicit calculations using the $t$ matrix of Love and Franey indicate that these effects play significant roles only for relatively large angles ($\theta \lesssim 60°$) and/or lower energies ($\sim 150$ MeV). These studies reinforce the conclusion that the lack of agreement between such first-order predictions and the data for spin observables at small angles arises from a physical effect not included in the nonrelativistic first-order theory, rather than from any uncertainty in the calculation or in its input.

## I. INTRODUCTION

The extraction of physically meaningful microscopic information from present-day high-quality elastic scattering data at intermediate energies is severely limited by the dominance of simple geometric aspects of the scattering which are described by any reasonable treatment of the first term of the multiple scattering expansion for the optical potential. This dominant geometry tends to mask our incomplete knowledge of the effective two-nucleon interaction and higher-order multiple scattering terms. The sought-after microscopic information which resides in the fine details of accurate data cannot be addressed with confidence unless the theoretical uncertainties in the dominant first-order theory of the optical potential are under precise control. Most implementations of first-order optical potential theories of the Kerman, McManus, and Thaler (KMT) type[1] have been carried out under a local, on-shell assumption in which the optical potential is described by $t(q)\rho(q)$, where $t(q)$ is the nucleon-nucleon (NN) $t$ matrix deduced from NN data, $\rho(q)$ is the nuclear density, and $q$ is the momentum transfer. The successes[2] of these treatments can be attributed in large part to the correct gross geometrical features of strength and range. The shortcomings[2] of these treatments, especially at energies below several hundred MeV or for spin-dependent observables, can arise from a variety of different sources, including higher-order terms in multiple scattering, relativistic dynamics, nuclear medium dependence of the NN interaction, and Pauli exchange effects. Not the least among the theoretical uncertainties is the reliability of the local, on-shell ansatz for the first-order multiple scattering term of the optical potential. In this paper we describe the details of a momentum-space formulation and calculations of elastic proton scattering due to a first-order microscopic optical potential. Results from investigations of the influence of off-shell and nonlocal effects are presented so that the theoretical ambiguities of the first-order theory as a function of energy, target mass, and scattering angle may be judged.

In this paper we focus entirely on the consideration of variants of the first-order nonrelativistic impulse approxi-

 

mation. Theoretical input to the calculations is restricted to the free $t_{NN}$ and to densities obtained from electron scattering. No adjustments or modifications arising from the sources already mentioned are made (relativistic effects are considered in separate papers). The motivation for such a careful examination of the (isolated) impulse approximation (IA) lies in the fact that it is the centerpiece of multiple scattering theories. Uncertainties and ambiguities which arise directly from the IA affect not only one's ability to extract physical implications from experimental data with the IA but also one's ability to ascertain the signature and the importance of relativistic effects, medium effects, etc. Of course, IA uncertainties are always present in addition to any ambiguities which arise from other sources. Thus it is crucially important to define sharply the range of variability inherent in predictions which rely strictly on the IA. Once the IA is carefully characterized, the investigation of other dynamical effects and the extraction of nuclear properties can be conducted with much greater confidence.

We choose a momentum-space representation for the calculations of the optical potential and for the solution of the elastic scattering equation primarily because the off-shell NN $t$ matrix arising from a realistic potential model is naturally defined in this representation. In the initial calculations[3] described and presented here, we do not employ such a general $t$ matrix but rather limit ourselves to the $t$ matrix of the Love and Franey model.[4] The closed-form expressions of this model simplify the computational tasks, while the on-shell values are realistic in that they are fitted to NN data and the off-shell extension is well defined. The computer code[5] WIZARD1, which we have developed for the nucleon-nucleus calculations, can accommodate a more general NN $t$ matrix. The momentum-space method is ideally suited to treating nonlocalities which arise in the microscopic optical potential without the need to find local equivalents or to adopt a local ansatz. Local prescriptions which turn out to be adequate for the description of elastic scattering data are not necessarily adequate for the complete description of the elastic wave function. Since the latter is needed for distorted wave calculations of inelastic scattering, we prefer to retain all nonlocal features of our microscopic optical potential with a view towards eventual use of the resulting elastic wave functions in calculations of other reactions.

The momentum-space treatment of proton elastic scattering employed in this work is similar in many respects to approaches to pion-nucleus elastic scattering. However, the important features of the pion case at intermediate energy, namely the resonant energy dependence and the dominance of a few angular momentum states of the two-body $t$ matrix, are replaced in the proton case by a weaker energy dependence, strong spin dependence, and a much larger range of momentum transfer and significant angular momentum components. In this work the first-order optical potential, expressed as the nuclear ground state matrix element of the NN $t$ matrix, is treated in the optimum factorization approximation following the manner recently employed for pions.[6] The nonlocalities and off-shell dependence predicted by this treatment derive from both the range and the energy dependence of the two-body $t$ matrix. In the pion case it is the nonlocality from the energy dependence which is the more important, while in the proton case it is the reverse. Much of our attention in this work is focused upon the range nonlocality of the $t$ matrix at a fixed two-body energy which is related to the beam energy.

A similar momentum-space formalism has been developed and applied to intermediate energy proton elastic scattering from $^4$He and $^3$He by Alexander and Landau and by Paez and Landau.[7] An on-shell NN $t$ matrix obtained from phase shift data and extended off shell through form factors obtained from a separable potential model is used in that work. The viability of that approach and the ability of first-order optical potential theory to reproduce the qualitative behavior of angular distributions from helium targets over a large range of scattering angles and beam energies is demonstrated in that work. Of particular note is the reproduction of back-angle peaks associated with exchange effects. This behavior *cannot* be obtained from local optical potentials constrained to behave like the nuclear density shape. The back-angle rise in the angular distribution from light nuclei is also found in our calculations for $^4$He, $^{12}$C, and $^{16}$O. The uncertainties in the NN $t$ matrix and nuclear density input and the factorization methods employed for the calculation of the first-order optical potential are found from our work to be largest for light nuclei and back angles. The need for exotic exchange mechanisms in explaining this phenomenon cannot be made in a convincing manner until the performance of the standard first-order theory is accurately documented. The results of our calculations suggest that for very light nuclei nothing less than a complete folding of a realistic off-shell $t$ matrix with the nuclear density matrix can settle this question. We note that for inelastic scattering at large angles[8] a strong sensitivity to the off-shell dependence of the effective NN $t$ matrix has been inferred from the comparison of results from several models based on NN data and modified to account for the influence of the nuclear medium.

The recent work on elastic scattering in which a Dirac formalism has been so successfully applied[9] further points up the need for the studies presented herein. In order to isolate the physical effect which accounts for the improved description of the data and to ensure ourselves of its unique identification, one must be able to eliminate other possible sources of effects of a similar character. This is one of the main thrusts of the present work.

In Sec. II we describe the optimum factorization treatment that we have employed for the first-order optical potential. We also describe several other factorized treatments that we have used to estimate the sensitivity to be expected from different approximate treatments of the full-folding integral. The expansion of the spin-dependent momentum-space optical potential in angular momentum states is given in Sec. III. We also describe the methods which are employed in various aspects of the calculations, including treatment of the Coulomb contribution to the optical potential and the treatment of high orbital angular momentum states. A discussion of results is contained in Sec. IV. A summary of the accomplishments of this paper is given in Sec. V.

## II. THE FIRST ORDER OPTICAL POTENTIAL

### A. Underlying theory

The Watson[10] multiple scattering series for the optical potential operator appropriate to the elastic scattering of a particle (0) from a bound state of $A$ particles can be written

$$U=\sum_{i=1}^{A}\tau_{0i}+\sum_{j\neq 1}^{A}\tau_{0i}QG_0\tau_{0j}+\cdots \ . \tag{2.1}$$

Here $G_0$ stands for $(E+i\delta-H_0)^{-1}$ which is the propagator for the noninteracting projectile-target system governed by the Hamiltonian $H_0$, which in turn is given as the sum of the projectile kinetic energy operator $K_0$ and the total Hamiltonian $H_A$ of the interacting target particles. The operator $Q$ projects onto the space spanned by all antisymmetric $A$-body eigenstates of $H_A$ except the ground state. The scattering operator $\tau_{0i}$ is given by

$$\tau_{0i}=v_{0i}+v_{0i}QG_0\tau_{0i} \ , \tag{2.2}$$

where $v_{0i}$ is an NN potential operator for interaction of particles (0) and ($i$).

The momentum-space optical potential matrix element is given by

$$U(\vec{k}',\vec{k})=\langle \vec{k}',\phi_0 \mid U \mid \phi_0,\vec{k}\rangle \ , \tag{2.3}$$

where $\mid \phi_0,\vec{k}\rangle$ stands for $\mid \phi_0\rangle \mid \vec{k}\rangle$ in which $\mid \phi_0\rangle$ is the ground state of the target nucleus and $\mid \vec{k}\rangle$ is the plane wave for the projectile in the zero momentum frame of the projectile plus nucleus system. If the position-space representation of the optical potential $U(\vec{r}',\vec{r})$ can be described by $\delta(\vec{r}'-\vec{r})U_L(\vec{r})$, then the calculation of the elastic scattering observables could proceed in the standard fashion from solutions of the Schrödinger differential equation. Since the microscopic description of $U$ yields, in general, a nonlocal optical potential, the required position-space wave equation is an integro-differential equation. Rather than take this approach to the calculations, we employ the momentum-space representation of the elastic scattering equation for the transition amplitude. This is the Lippmann-Schwinger integral equation, which is

$$T(\vec{k}',\vec{k})=U(\vec{k}',\vec{k})+\int d^3k''\frac{U(\vec{k}',\vec{k}'')T(\vec{k}'',\vec{k})}{E(k)+i\delta-E(k'')} \ , \tag{2.4}$$

where $\vec{k}$ is the initial (on-shell) momentum and $E(k)$ is the corresponding initial energy of the system. The principal advantage of performing the calculation in this manner is that one is not hampered by the necessity of devising approximate treatments of the microscopic theory of the optical potential which lead to manageable, but questionable, forms for $U$ in the position space representation. Additional advantages include the simple incorporation of relativistic kinematics and recoil.

We here restrict our attention to the first-order multiple scattering term for the optical potential. That is, we take

$$U(\vec{k}',\vec{k})\approx U^{(1)}(\vec{k}',\vec{k})=A\langle \vec{k}',\phi_0 \mid \tau \mid \phi_0,\vec{k}\rangle \ , \tag{2.5}$$

where $\tau$ is any one of the $\tau_{0i}$, and we have used the antisymmetric character of $\mid \phi_0\rangle$. To relate the operator $\tau$ to the $t$ matrix, which represents the solution of the problem of the scattering of two nucleons, we express Eq. (2.2) in the form

$$\tau_{0i}=\tilde{t}_{0i}-\tilde{t}_{0i}PG_0\tau_{0i} \ , \tag{2.6}$$

where

$$\tilde{t}_{0i}=v_{0i}+v_{0i}\mathscr{A}G_0\tilde{t}_{0i} \tag{2.7}$$

and the projector $P$ stands for $\mid \phi_0\rangle\langle \phi_0 \mid$ which is related to $Q$ by $P=\mathscr{A}-Q$, where $\mathscr{A}$ is the projector onto the complete, antisymmetric space of the target nucleons. The operator $\tilde{t}_{0i}$ is presumably much more readily approximated by the free NN $t$ matrix $t_{0i}^F$ than is $\tau_{0i}$.

A supporting argument for this assertion is as follows. For ground state target expectation values, such as the one in Eq. (2.5), the important plane wave matrix elements of the operator for scattering of the projectile from a bound nucleon are those in which very little momentum is transferred to the bound nucleon. These momentum states of the bound nucleon have a large overlap with the nuclear ground state [this can be verified from Eq. (2.26) given later on]. If the free N-N $t$ matrix $t_{0i}^F$ were to be used in Eq. (2.5), then intermediate states in which one nucleon has a large overlap with the single particle states of the target would be favored. The intermediate state structure of the operator $\tilde{t}_{0i}$, given by Eq. (2.7), is such that this would also be the case were $\tilde{t}_{0i}$ to be used in Eq. (2.5) since $\mathscr{A}\mid \phi_0\rangle=\mid \phi_0\rangle$. The Watson operator $\tau_{0i}$, on the other hand, has the target ground state explicitly prohibited from the intermediate state spectrum because of the operator $Q$ and is therefore not so readily approximated by the free $t$.

The first order KMT prescription is equivalent to the approximation $\tilde{t}_{0i}\approx t_{0i}^F$ with $\tau_{0i}$ calculated from Eq. (2.6) and $U^{(1)}(k',k)$ from Eq. (2.5), without further approximation. We will comment on the above-mentioned approximation shortly. The target ground state matrix elements of $\tau_{0i}$ do not have to be calculated explicitly since, upon taking the relevant matrix elements, Eq. (2.6) takes on the same form as the integral equation for the elastic scattering amplitude $T(\vec{k}',\vec{k})$ given in Eq. (2.4). The combination of the three equations (2.4), (2.5), and (2.6) yields the familiar first-order KMT formulation in which the elastic scattering amplitude is given by

$$T(\vec{k}',\vec{k})=\frac{A}{A-1}\hat{T}(\vec{k}',\vec{k}) \ , \tag{2.8}$$

where the auxiliary elastic amplitude is determined by the solution of the integral equation

$$\hat{T}(\vec{k}',\vec{k})=\hat{U}^{(1)}(\vec{k}',\vec{k})+\int d^3k''\frac{\hat{U}^{(1)}(\vec{k}',\vec{k}'')\hat{T}(\vec{k}'',\vec{k})}{E(k)+i\delta-E(k'')} \ , \tag{2.9}$$

and the auxiliary first order optical potential is defined by

$$\hat{U}^{(1)}(\vec{k}',\vec{k})=(A-1)\langle \vec{k}',\phi_0 \mid \tilde{t} \mid \phi_0,\vec{k}\rangle \ , \tag{2.10}$$

where $\tilde{t}$ is any one of the $\tilde{t}_{0i}$. Since the operator $\tilde{t}_{0i}$ contains no restriction (other than antisymmetry of the target nucleons) on the allowed intermediate states, the auxiliary optical potential $\hat{U}^{(1)}$ contains contributions from intermediate states in which the target propagates in its ground state. We emphasize that these contributions are not spurious since they are not present in the true (Watson) optical potential which is the equivalent of the above-mentioned KMT formulation and which is given by Eq. (2.5). We also note that, although an approximation of $\tilde{t}_{0i}$ in Eq. (2.10) by the free-space NN $t$ matrix $t^F_{0i}$ ignores nuclear medium modifications of the NN scattering amplitude contained in the definition of the auxiliary KMT optical potential $\hat{U}^{(1)}$, it does not ignore nuclear medium modifications of the effective NN scattering operator ($\tau$) used in describing the equivalent physical (Watson) optical potential. For example, if $\tilde{t}_{0i}$ were taken to be the free NN $t$ matrix and an infinite nuclear matter model employed for the description of the target in the propagator of the second term of Eq. (2.6), then $\tau_{0i}$ would reduce essentially to the Brueckner-Bethe-Goldstone[11] $g$ matrix for the scattering interaction of a distinguishable particle from a nucleon constituent of nuclear matter. This is because the ground state projector $P$ becomes, in this limit, the projector onto the interior of the Fermi momentum sphere. If the relation $k_F(\rho_m)$ between Fermi momentum $k_F$ and nuclear matter density $\rho_m$ were to be used with the local density approximation $\rho_m \to \rho(r)$ for a finite-sized nucleus, then Eq. (2.6) can be expected to contain a substantial overlap with the content of these approaches. For a nucleon projectile, a feature of the local density $g$-matrix approach that is not contained in Eq. (2.6) is the antisymmetrization of the projectile with respect to the target nucleons. In this work we have not as yet addressed the identity of the projectile in the description of the theory underlying our approach. We adopt the approach of Picklesimer and Thaler[12] in this matter, who show that it is possible to develop a multiple scattering expansion in the case where the projectile is identical with the target nucleons by distributing, in an exact way, the Pauli exchanges involving the projectile amongst all terms of the multiple scattering expansion so that in each term the identity of all the "active" particles experiencing the residual interaction is respected. For the first-order multiple scattering term, this formulation leads to the same expression as given in Eq. (2.10) for the auxiliary KMT optical potential, with the requirement that $\tilde{t}_{0i}$ be antisymmetrized with respect to exchange of the projectile with just particle ($i$) of the target. This result and its extension to higher-order multiple scattering terms is a confirmation of the validity of the prescription advocated by Takeda and Watson[13] and by KMT. It is a physically reasonable approach for high energy scattering. For low energies it may be more appropriate to retain the full restrictions of $(A+1)$ body antisymmetry in each term of a multiple scattering expansion.[14] In this way a nucleon-nucleon scattering operator having features very close to those of a finite nucleus $g$ matrix would be obtained for use in a first-order optical potential. However, there would remain residual differences due to the fact that the definition of the standard $g$ matrix originates from bound state perturbation theory in which the zeroth-order Hamiltonian is symmetric in the coordinates of all particles in the system. In the scattering case the corresponding Hamiltonian is the asymptotic channel Hamiltonian which, by its very nature, is necessarily not symmetric in all $A+1$ body coordinates. An antisymmetric multiple scattering model incorporating these considerations is being developed and investigations of the first-order term are in progress.[15]

The calculations described in this paper utilize Eqs. (2.8)—(2.10) together with the assumption that $\tilde{t}$ in Eq. (2.10) may be replaced by $t^F$, the antisymmetric free NN $t$ matrix. Since $\tilde{t}_{0i}$ is a many-body operator due to the many-body nature of both $\mathscr{A}$ and $G_0$ in Eq. (2.7), the validity of this assumption is difficult to judge. At the very least a three-body model is needed to investigate this point, as well as to fix a suitable prescription for the effective NN energy at which the free NN $t$ matrix employed should be evaluated. We do not investigate these questions in this work. We choose a reasonable prescription for the energy parameter of the free NN $t$ matrix and consider the consequences of various factorization prescriptions for the evaluation of Eq. (2.10) and the consequent influence on the scattering observables.

### B. Optimum factorization

In the remainder of this paper we will deal only with the first-order optical potential within the KMT formulation and therefore omit the superscript denoting first order from Eqs. (2.9) and (2.10). The problem at hand is described in the zero momentum frame of the nucleon-nucleus system by

$$\hat{T}(\vec{k}',\vec{k})=\hat{U}(\vec{k}',\vec{k})+\int d^3k''\frac{\hat{U}(\vec{k}',\vec{k}'')\hat{T}(\vec{k}'',\vec{k})}{E(k)+i\delta-E(k'')}\ , \tag{2.11}$$

where

$$\hat{U}(\vec{k}',\vec{k})=(A-1)\langle \vec{k}',\phi_0 \mid t(\epsilon) \mid \phi_0,\vec{k}\rangle\ . \tag{2.12}$$

Here $t(\epsilon)$ is the free NN $t$ matrix evaluated at a fixed energy $\epsilon$ to be specified shortly. In Eq. (2.12) the integrations over the initial and final momenta of the struck nucleon of the target are reduced to one momentum integration through conservation of total two-nucleon momentum obeyed by the operator $t(\epsilon)$. That is, through the use of the relation

$$\langle \vec{k}';\vec{k}'_1 \mid t(\epsilon) \mid \vec{k};\vec{k}_1\rangle=\delta(\vec{k}'+\vec{k}'_1-\vec{k}-\vec{k}_1)\langle \vec{k}';\vec{k}'_1 \mid t(\epsilon) \mid \vec{k};\vec{k}_1\rangle\ , \tag{2.13}$$

with the introduction of the variables $\vec{q}=\vec{k}'-\vec{k}$, $\vec{K}=\frac{1}{2}(\vec{k}'+\vec{k})$, and $\vec{p}=\vec{k}_1-\frac{1}{2}\vec{q}$, Eq. (2.10), when expressed with kinematics that maintain time reversal invariance, becomes

$$\hat{U}(\vec{k}',\vec{k})=(A-1)\int d^3p\sum_{s,i}\langle\vec{k}';\vec{p}-\tfrac{1}{2}\vec{q},s,i\,|\,t(\epsilon)\,|\,\vec{k};\vec{p}+\tfrac{1}{2}\vec{q},s,i\rangle\rho^{s,i}_{\rm int}[\vec{m}\,'(\vec{p},\vec{q},\vec{K});\vec{m}(\vec{p},\vec{q},\vec{K})]\ , \tag{2.14}$$

where

$$\vec{m}\,'=\vec{p}-\frac{A-1}{A}\frac{\vec{q}}{2}+\frac{\vec{K}}{A};\quad \vec{m}=\vec{p}+\frac{A-1}{A}\frac{\vec{q}}{2}+\frac{\vec{K}}{A}\ . \tag{2.15}$$

In Eq. (2.14), $s$ and $i$ are the spin and isospin projections of the struck nucleon which must be conserved for elastic scattering, and $\hat{U}(\vec{k}',\vec{k})$ and the matrix element of $t(\epsilon)$ are operators in the spin and isospin space of the projectile nucleon. The quantity $\rho^{s,i}_{\rm int}(\vec{m}\,';\vec{m})$ is the one-nucleon density matrix of the target corresponding to a change in the intrinsic momentum from $\vec{m}$ to $\vec{m}\,'$ for a nucleon of spin and isospin projections $s,i$. By intrinsic momentum we mean the momentum of a nucleon relative to the center of mass of the remaining nucleons (core). To simplify matters, we assume that we are dealing with a spin-saturated nucleus, i.e., $\rho^{s,i}_{\rm int}(\vec{m}\,';m)=\rho^{s',i}_{\rm int}(\vec{m}\,';\vec{m})=\rho^{i}_{\rm int}(\vec{m}\,';\vec{m})$. In this circumstance, the spin trace will eliminate those components of the $t$ matrix which depend (linearly) on the spin of the struck nucleon. The eliminated terms are the tensor term, and the $\vec{\sigma}_1\cdot\vec{\sigma}_2$ and $\vec{\sigma}_1\cdot\vec{\sigma}_2\vec{\tau}_1\cdot\vec{\tau}_2$ parts of the central term. The remaining terms are the spin-independent central term and part of the spin-orbit term for each of the pp and np $t$ matrices. We denote these "reduced" $t$ matrices by $t'_\alpha$ and the corresponding density matrix by $\rho^\alpha_{\rm int}$ where $\alpha=$n,p.

Thus far we have for a proton projectile

$$\hat{U}(\vec{k}',\vec{k})=\frac{A-1}{A}\sum_{\alpha=\rm n,p}\int d^3p\langle\vec{k}';\vec{p}-\tfrac{1}{2}\vec{q}\,|\,t'_\alpha(\epsilon)\,|\,\vec{k};\vec{p}+\tfrac{1}{2}\vec{q}\rangle\rho^\alpha_{\rm int}(\vec{m}\,';\vec{m})\ , \tag{2.16}$$

where the density matrices are normalized to $N$ for neutrons and $Z$ for protons. It is convenient to make a change of integration variable from $\vec{p}$ to $\vec{P}=\vec{p}+(\vec{K}/A)$, so that Eq. (2.16) becomes

$$\hat{U}(\vec{k}',\vec{k})=\frac{A-1}{A}\sum_{\alpha=\rm n,p}\int d^3P\left\langle\vec{k}';\vec{P}-\frac{\vec{q}}{2}-\frac{\vec{K}}{A}\left|t'_\alpha(\epsilon)\right|\vec{k};\vec{P}+\frac{\vec{q}}{2}-\frac{\vec{K}}{A}\right\rangle\rho^\alpha_{\rm int}\left[\vec{P}-\gamma\frac{\vec{q}}{2};\vec{P}+\gamma\frac{\vec{q}}{2}\right]\ , \tag{2.17}$$

where $\gamma=(A-1)/A$. We note that the density matrix is related to the momentum-space density profile $\rho^\alpha(q)$ of the nucleus by

$$\rho^\alpha(q)\equiv\rho^\alpha_{\rm int}\left[\frac{A-1}{A}q\right]=\int d^3P\,\rho^\alpha_{\rm int}\left[\vec{P}-\frac{A-1}{A}\frac{\vec{q}}{2};\vec{P}+\frac{A-1}{A}\frac{\vec{q}}{2}\right]\ , \tag{2.18}$$

where $\rho^\alpha(q)$ is the Fourier transform of the position space point neutron or point proton density profile defined in a system of coordinates with the origin at the center of mass of the nucleus. The normalization is such that $\rho^\alpha(q=0)=N$ or $Z$. If $\vec{q}$ is the momentum transfer taken up by the degree of freedom described by the position $\vec{R}$ of the struck nucleon relative to the center of mass of the target, then $(A-1/A)\vec{q}$ is the momentum transfer taken up by the degree of freedom described by the position $\vec{r}=(A/A-1)\vec{R}$ of the struck nucleon relative to the center of mass of the core. We will deal with the density $\rho^\alpha(q)$, since for protons it can be obtained from the nuclear charge density measured by electron scattering after the intrinsic proton charge form factor is divided out. We will take the point neutron density to be equal to the point proton density for $N=Z$ nuclei unless otherwise stated. This is expected to be a good approximation for $N=Z$ nuclei.

The NN $t$-matrix element in Eq. (2.17) is evaluated in the zero-momentum frame of the nucleon-nucleus system. The relationship to the corresponding $t$-matrix element evaluated in the zero-momentum frame of the two nucleons is taken to be

$$\left\langle\vec{k}';\vec{P}-\frac{\vec{q}}{2}-\frac{\vec{K}}{A}\left|t'_\alpha(\epsilon)\right|\vec{k};\vec{P}+\frac{\vec{q}}{2}-\frac{\vec{K}}{A}\right\rangle_{NA}=\eta(\vec{P},\vec{q},\vec{K})\langle\vec{\kappa}\,'\,|\,t'_\alpha(\epsilon)\,|\,\vec{\kappa}\rangle_{\rm NN}\ , \tag{2.19}$$

where the initial nucleon momentum $\vec{\kappa}$ and the final nucleon momentum $\vec{\kappa}\,'$ in the zero momentum frame of the NN system are taken to be given by the nonrelativistic definitions

$$\vec{\kappa}=\tfrac{1}{2}\left[\vec{k}-\left[\vec{P}+\frac{\vec{q}}{2}-\frac{\vec{K}}{A}\right]\right] \tag{2.20}$$

and

$$\vec{\kappa}\,'=\tfrac{1}{2}\left[\vec{k}\,'-\left[\vec{P}-\frac{\vec{q}}{2}-\frac{\vec{K}}{A}\right]\right]\ . \tag{2.21}$$

The first factor $\eta$ in Eq. (2.19) is the Möller[16] factor for the frame transformation and is given by

$$\eta(\vec{P},\vec{q},\vec{K})=\left[\frac{E_{\rm N}(\vec{\kappa}\,')E_{\rm N}(-\vec{\kappa}\,')E_{\rm N}(\vec{\kappa})E_{\rm N}(-\vec{\kappa})}{E_{\rm N}(\vec{k}\,')E_{\rm N}\left[\vec{P}-\frac{\vec{q}}{2}-\frac{\vec{K}}{A}\right]E_{\rm N}(\vec{k})E_{\rm N}\left[\vec{P}+\frac{\vec{q}}{2}-\frac{\vec{K}}{A}\right]}\right]^{1/2}\ , \tag{2.22}$$

where $E_N(\vec{k})$ is the (relativistic) energy of a nucleon of momentum $\vec{k}$. This factor imposes the Lorentz invariance of flux. The NN $t$ matrix on the right-hand side of Eq. (2.19) can be written in the form

$$\langle \vec{k}' | t'_\alpha(\epsilon) | \vec{k} \rangle_{NN} = t'_\alpha(\epsilon;\vec{q},2\vec{\mathcal{K}}) , \tag{2.23}$$

where

$$\vec{q}=\vec{k}'-\vec{k}=\vec{k}'-\vec{k} \tag{2.24}$$

and

$$\vec{\mathcal{K}}(\vec{P})=\tfrac{1}{2}(\vec{k}'+\vec{k})=\frac{1}{2}\left[\frac{A+1}{A}\vec{K}-\vec{P}\right] . \tag{2.25}$$

This form is useful since the roles of the variables $\vec{q}$ and $2\vec{\mathcal{K}}$ are reversed in a spatial exchange operation. The model of the NN $t$ matrix that we employ is specified in terms of its dependence on $\vec{q}$ and $2\vec{\mathcal{K}}$. With these notations, Eq. (2.17) becomes

$$\hat{U}(\vec{k}',\vec{k})=\frac{A-1}{A}\sum_{\alpha=n,p}\int d^3P\,\eta(\vec{P},\vec{q},\vec{K})t'_\alpha[\epsilon;\vec{q},2\vec{\mathcal{K}}(\vec{P})] \times\rho^\alpha_{int}\left[\vec{P}-\gamma\frac{\vec{q}}{2};\vec{P}+\gamma\frac{\vec{q}}{2}\right] . \tag{2.26}$$

This "full-folding" expression for the first-order KMT optical potential is numerically quite difficult to compute and to our knowledge no microscopic treatment of proton elastic scattering which fully incorporates this integral has been reported. Most treatments have adopted a local form (independent of $\mathcal{K}$) for the NN $t$ matrix. This leads to a $t(q)\rho(q)$ structure in which the equivalent convolution integral in position space has effectively been performed. In this work we employ the optimum factorization approximation for Eq. (2.26). Since the nuclear size is significantly larger than the range of the NN interaction, and therefore also of the $t$ matrix (if the energy parameter is fixed), the most slowly varying factor in Eq. (2.26) is $\eta t'_\alpha$. The method of optimum factorization is to expand $\eta t'_\alpha$ in a Taylor series in $\vec{P}$ about a fixed value $\vec{P}_0$, which is chosen by requiring that the contribution of the first derivative term is minimized. The expansion

$$\eta(\vec{P})t'_\alpha(\vec{P})=\eta(\vec{P}_0)t'_\alpha(\vec{P}_0) +(\vec{P}-\vec{P}_0)\cdot\partial_{\vec{P}_0}\eta(\vec{P}_0)t'_\alpha(\vec{P}_0)+\cdots \tag{2.27}$$

when used in Eq. (2.26) gives

$$\hat{U}(\vec{k}',\vec{k})=\frac{A-1}{A}\eta(\vec{P}_0,\vec{q},\vec{K})\sum_{\alpha=n,p}t'_\alpha[\epsilon;\vec{q},2\vec{\mathcal{K}}(\vec{P}_0)] \times\rho^\alpha(q)+\Delta\hat{U}+\cdots , \tag{2.28}$$

where

$$\Delta\hat{U}=\frac{A-1}{A}\sum_{\alpha=n,p}[\partial_{\vec{P}_0}\eta(\vec{P}_0)t'_\alpha(\vec{P}_0)] \times\int d^3P(\vec{P}-\vec{P}_0)\rho^\alpha_{int}\left[\vec{P}-\gamma\frac{\vec{q}}{2};\vec{P}+\gamma\frac{\vec{q}}{2}\right] . \tag{2.29}$$

The time-reversal invariance property of the ground state density matrix for even-even nuclei leads to

$$\int d^3P\,\vec{P}\rho^\alpha_{int}\left[\vec{P}-\gamma\frac{\vec{q}}{2};\vec{P}+\gamma\frac{\vec{q}}{2}\right]=0 \tag{2.30}$$

so that $\Delta\hat{U}$ is zero if we choose $\vec{P}_0=0$. Thus the optimally factorized optical potential is

$$\hat{U}(\vec{k}',\vec{k})=\frac{A-1}{A}\eta(\vec{q},\vec{K})\sum_{\alpha=n,p}t'_\alpha\left[\epsilon;\vec{q},\frac{A+1}{A}\vec{K}\right]\rho^\alpha(q) , \tag{2.31}$$

where $\eta(\vec{q},\vec{K})$ shall be used to stand for $\eta(\vec{P}=0,\vec{q},\vec{K})$. Referring back to Eq. (2.19), we see that the optimum choice for factorization, $\vec{P}=0$, selects the initial momentum of the struck nucleon to be $(\vec{q}/2)-(\vec{K}/A)$ and the final momentum to be $-(\vec{q}/2)-(\vec{K}/A)$ in the frame of zero total momentum of the system. This is illustrated pictorially in Fig. 1. In the limit of a single nucleon for the target ($A=1$), these momenta become $-\vec{k}$ and $-\vec{k}'$, which are the correct values for NN scattering. Also, in this limit, $\eta\to 1$ and $\rho^\alpha(q)\to 1$. In the general case, the recoil effects for a finite target mass are included through the kinematics employed in Eq. (2.31).

The optical potential obtained thus far is an operator in the spin space of the projectile. To make the spin dependence explicit we write the $t$ matrix $t'_\alpha$ (which has been averaged over the spin of the struck nucleon) in the form

$$t'_\alpha(\epsilon;\vec{q},2\vec{\mathcal{K}})=t^c_\alpha(\epsilon;\vec{q},2\vec{\mathcal{K}})+\frac{i}{2}\vec{\sigma}\cdot\vec{q}\times\vec{\mathcal{K}}t^{LS}_\alpha(\epsilon;\vec{q},2\vec{\mathcal{K}}) . \tag{2.32}$$

The first term corresponds to the central spin-independent contribution, while the second term corresponds to the spin-orbit contribution. In the latter term the usual total Pauli spin operator of the NN system is replaced by just the projectile's Pauli spin operator, the other having been eliminated by the trace over the spin of the struck nucleon. With an on-shell constraint, $t^c_\alpha$ for $\alpha=n,p$ is proportional to the NN Wolfenstein[17] spin-independent

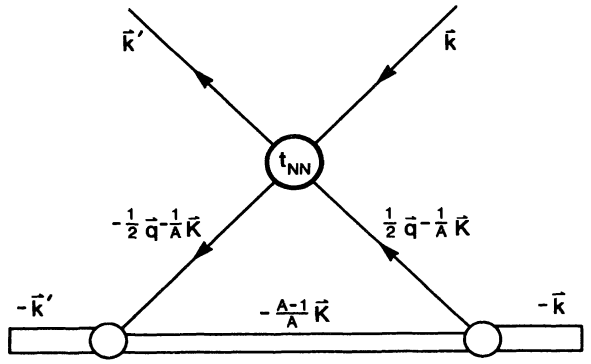


FIG. 1. The first order term in the optical potential. The diagram illustrates the kinematics in the zero total momentum frame implied by "optimum" factorization. Here $\vec{q}=(\vec{k}'-\vec{k})$ and $\vec{K}=\frac{1}{2}(\vec{k}'+\vec{k})$.

scattering amplitudes $A_{pn}(q)$ and $A_{pp}(q)$, respectively, while $t_\alpha^{LS}$, for $\alpha=$n,p, is proportional to the NN Wolfenstein spin-dependent scattering amplitudes $C_{pn}(q)$ and $C_{pp}(q)$, respectively. Substitution of Eq. (2.32) into Eq. (2.31) gives the optical potential as

$$\hat{U}(\vec{k}',\vec{k})=\hat{U}^c(\vec{k}',\vec{k})+\frac{i}{2}\vec{\sigma}\cdot\vec{q}\times\vec{K}\hat{U}^{LS}(\vec{k}',\vec{k}) , \tag{2.33}$$

where the central term is given by

$$\hat{U}^c(\vec{k}',\vec{k})=\frac{A-1}{A}\eta(\vec{q},\vec{K})\sum_{\alpha=n,p}t_\alpha^c\left[\epsilon;\vec{q},\frac{A+1}{A}\vec{K}\right]\rho^\alpha(q) , \tag{2.34}$$

and the spin-orbit term is given by

$$\hat{U}^{LS}(\vec{k}',\vec{k})=\frac{A-1}{A}\eta(\vec{q},\vec{K})\left[\frac{A+1}{2A}\right]\times\sum_{\alpha=n,p}t_\alpha^{LS}\left[\epsilon;\vec{q},\frac{A+1}{A}\vec{K}\right]\rho^\alpha(q) . \tag{2.35}$$

Equations (2.33)—(2.35) exhibit the nonlocality and off-shell effects present in the optimally factorized optical potential. The nonlocality is evident in the dependence of $\eta$ and $t_\alpha$ upon $\vec{K}=\frac{1}{2}(\vec{k}'+\vec{k})$. The factor $(i/2)\vec{\sigma}\cdot(\vec{q}\times\vec{K})$ comes from the momentum representation of the spin-orbit operator $\vec{L}\cdot\vec{S}$ and is always included in optical potentials which are referred to as local. The off-shell effects enter in Eqs. (2.34) and (2.35) because the three arguments of $t_\alpha^c$ and $t_\alpha^{LS}$ are completely independent. Inspection of Eqs. (2.23)—(2.25) shows that the imposition of the two-body, on shell constraint $|\vec{\kappa}'|=|\vec{\kappa}|$ and $\epsilon=E_N(\vec{\kappa})+E_N(-\vec{\kappa})$ in terms of the variables $\vec{q}$ and $\vec{K}$ leads to

$$\vec{q}\cdot\vec{K}=0 , \tag{2.36}$$

$$q^2+\left[\frac{A+1}{A}K\right]^2=4\kappa^2 , \tag{2.37}$$

where $\vec{\kappa}$ is the on-shell nucleon momentum in the zero momentum frame of the NN system and is calculated from the prescribed value of $\epsilon$. Thus, under the on-shell constraints, the third argument $[(A+1/A)\vec{K}]$ of the $t$ matrices in Eqs. (2.34) and (2.35) is completely determined by $\epsilon$ and $\vec{q}$ and the optical potential becomes local, apart from the nonlocality of the Möller factor $\eta(\vec{q},\vec{K})$. This latter nonlocality is found to be quite negligible. In the calculations employing the optimally factorized optical potential we have made use of the Love-Franey[4] model of $t_{NN}$ in which the $t_\alpha^c$ and $t_\alpha^{LS}$ can be obtained as functions of the three independent variables as required in Eqs. (2.34) and (2.35). The energy parameter $\epsilon$ of the $t$ matrix is taken to be fixed at the value appropriate to NN scattering at a laboratory energy equal to the beam energy. This prescription ignores recoil energy shifts and should be most appropriate for forward angle nucleon-nucleus scattering, assuming that binding energy shifts are not important. As discussed later, we have estimated the error in this prescription and find it to be quite small. The resemblance of the off-shell behavior inherent in this $t$-matrix model with that obtained for $t$ matrices generated from phenomenological potentials is not known. We view the obtained nucleon-nucleus results as including typical off-shell effects related to the range of the interaction.

### C. Other factorizations

We will compare the nucleon elastic scattering results from the optimally factorized optical potential with results from several other factorizations which treat off shell and nonlocalities in a different way. These comparisons are used to estimate the influence of these effects and to judge the departures from the optimum factorization results that might be obtained if the folding integral in Eq. (2.26) were to be computed exactly.

The usual on-shell factorized optical potential can be obtained from Eqs. (2.34) and (2.35) by fixing the third argument of the $t$-matrix components $t_\alpha^c$ and $t_\alpha^{LS}$ in terms of $\epsilon$ and $\vec{q}$ by using Eqs. (2.36) and (2.37). We write the resulting $t$-matrix components as $t_\alpha^c(\epsilon;\vec{q})$ and $t_\alpha^{LS}(\epsilon;\vec{q})$. For this prescription, which we refer to as OS1, the central and spin-orbit optical potentials are

$$\hat{U}^c_{OS1}(\vec{k}',\vec{k})=\frac{A-1}{A}\eta\sum_{\alpha=n,p}t_\alpha^c(\epsilon;\vec{q})\rho^\alpha(q) \tag{2.38}$$

and

$$\hat{U}^{LS}_{OS1}(\vec{k}',\vec{k})=\frac{A-1}{A}\eta\left[\frac{A+1}{2A}\right]\sum_{\alpha=n,p}t_\alpha^{LS}(\epsilon;\vec{q})\rho^\alpha(q) . \tag{2.39}$$

We have ignored here the very small effects from the momentum dependence of $\eta$. This optical potential is local and corresponds to the prescription used for most previous intermediate energy calculations referred to in the literature as employing the first-order KMT theory. The on-shell $t$-matrix components in Eqs. (2.38) and (2.39) can be obtained directly from compilations of NN phase shift data.[17] The utility of this OS1 prescription decreases with decreasing energy because the range of momentum transfer over which an on-shell NN $t$ matrix exists is significantly less than the range of momentum transfer accessible in nucleon-nucleus scattering. With the NN energy $\epsilon$ fixed at the value appropriate to NN scattering at the beam energy, the on-shell NN relative momentum is approximately half of the on-shell nucleon-nucleus momentum for a heavy target. Thus, at a nucleon-nucleus scattering angle of approximately 60°, the NN $t$-matrix components in Eqs. (2.38) and (2.39) correspond to an NN scattering angle of 180°. The nuclear form factor beyond 60° nuclear scattering at high energies is sufficiently small so as to mask contributions to the small angle scattering amplitude from large momentum transfer components of the optical potential. The OS1 prescription can be expected to be adequate for descriptions of scattering data in the forward hemisphere. At lower energies and/or for light nuclei where nuclear scattering data can be measured in the backward hemisphere, the OS1 prescription can be expected to be inadequate. The calculations that we present in Sec. IV confirm these expectations. In our implemen-

tation of the OS1 prescription we set the optical potential to zero for momentum transfers beyond which the on-shell $t$ matrix does not exist. Of course, this extreme method of dealing with the optical potential outside the region where the on-shell $t$ matrix exists is unphysical. However, we use the OS1 results solely to identify the regions of momentum transfer, beam energy, and target mass, where the limitations of the completely on-shell factorization show up *at all*. The optimum factorization method provides results which do not have these limitations and which are on a better theoretical foundation.

A second on-shell factorization prescription (OS2) with which we compare is similar to OS1 discussed previously, with the exception that the NN relative energy parameter $\epsilon$ of the on-shell $t$ matrix $t(\epsilon;\vec{q})$ is calculated from the invariant mass of the NN system defined by the kinematics shown in Fig. 1. This prescription for the energy of the NN $t$ matrix has been suggested by studies in which the many-body propagator $G_0$ of Eq. (2.7) is expanded about the two-nucleon propagator $g_0(\epsilon)$ which would make the operator $\tilde{t}_{0i}$ in Eq. (2.7) the free NN $t$ matrix. The effects of the first-order correction $[G_0-g_0(\epsilon)]$ can be argued to be minimal when $\epsilon$ is calculated from the invariant NN mass.[18]

From Fig. 1, the square of the invariant mass is

$$\epsilon^2=S_{\rm NN}=\left[E_{\rm N}(\vec{k})+E_{\rm N}\left[\tfrac{1}{2}\vec{q}-\frac{1}{A}\vec{K}\right]\right]^2-\left[\frac{A-1}{A}K\right]^2, \tag{2.40}$$

where $E_{\rm N}^2(k)=k^2+m_{\rm N}^2$. With the on-shell constraint $\vec{q}\cdot\vec{K}=0$, the NN $t$-matrix total energy $\epsilon$ defined this way is a function of target mass number $A$, on-shell nucleon-nucleus momentum $k$, and momentum transfer $q$, and is given by

$$\epsilon^2(A,k,q)=\left\{(k^2+m_{\rm N}^2)^{1/2}+\left[\tfrac{1}{4}q^2\left[1-\frac{1}{A^2}\right]+\frac{1}{A^2}k^2+m_{\rm N}^2\right]^{1/2}\right\}^2-(k^2-\tfrac{1}{4}q^2)\left[1-\frac{1}{A}\right]^2. \tag{2.41}$$

When $q=2k$, we obtain

$$\epsilon(A,k,q=2k)=2E_{\rm N}(k) \tag{2.42}$$

so that the NN system on-shell momentum becomes equal to the nucleon-nucleus (N$A$) system on-shell momentum and the 180° scattering conditions coincide for the NN and N$A$ systems. Thus, with this variable-energy on-shell prescription for the $t$ matrix, the OS2 optical potential is defined for all momentum transfers accessible in on-shell nuclear scattering. Of course, in solving the Lippmann-Schwinger equation, the optical potential is required for larger momentum transfers, but the nuclear form factor causes such contributions to be quite negligible. For the OS2 prescription we have set the optical potential to be zero beyond this momentum transfer where the on-shell $t$ matrix is not defined. Comparison of the results obtained from the OS2 optical potential to the results obtained from the optimally factorized optical potential provides an estimation of the effects which generally arise from coupling the $t$-matrix energy to the kinematics of the first-order optical potential reaction mechanism. Also, since this prescription is local, a comparison to the optimum factorization results provides a sensible estimation of the role played by the nonlocality in the latter prescription.

The final variation that we consider for the factorization of the optical potential is the asymptotic momentum (ASM) approximation which has been found to be qualitatively reasonable for distorted-wave impulse approximation (DWIA) treatments of inelastic scattering.[19] In this approximation the nonlocality variable $\vec{K}$ of the $t$-matrix components in Eqs. (2.34) and (2.35) is replaced by its (fixed) limiting value $\vec{k}_0$ which is appropriate for forward angle on-shell scattering. The resulting optical potential is (like prescriptions OS1 and OS2) local, but some off-shell effects are retained.

## III. CALCULATIONAL FRAMEWORK

### A. Partial wave expressions

The optimally factorized first-order KMT optical potential as an operator in the spin space of the projectile is given in Eq. (2.33) as

$$\hat{U}(\vec{k}',\vec{k})=\hat{U}^c(\vec{k}',\vec{k})+\frac{i}{2}\vec{\sigma}\cdot\vec{q}\times\vec{K}\hat{U}^{LS}(\vec{k}',\vec{k}). \tag{3.1}$$

From conservation of total angular momentum and parity, this spin operator can be expanded as

$$\hat{U}(\vec{k}',\vec{k})=4\pi\sum_{JLM}\mathscr{Y}_{JL}^{M}(\hat{k}')\hat{U}_{LJ}(k',k)\mathscr{Y}_{JL}^{M\dagger}(\hat{k}), \tag{3.2}$$

where $J=L\pm\frac{1}{2}$ and

$$\mathscr{Y}_{JL}^{M}(\hat{k})=\sum_{M_L,m_S}Y_L^{M_l}(\hat{k})\,|\,m_s\rangle\langle Lm_L;\tfrac{1}{2}m_S\,|\,JM\rangle \tag{3.3}$$

is a standard spin-spherical harmonic. When the expansion in Eq. (3.2) is substituted into the Lippmann-Schwinger equation [Eq. (2.11)], the resulting transition operator for elastic scattering is seen to have the analogous expansion

$$\hat{T}(\vec{k}',\vec{k})=4\pi\sum_{JLM}\mathscr{Y}_{JL}^{M}(\hat{k}')\hat{T}_{LJ}(k',k)\mathscr{Y}_{JL}^{M\dagger}(\hat{k}), \tag{3.4}$$

with the components satisfying

$$\hat{T}_{LJ}(k',k)=\hat{U}_{LJ}(k',k)+4\pi\int_0^\infty k''^2dk''\frac{\hat{U}_{LJ}(k',k'')\hat{T}_{LJ}(k'',k)}{E(k)+i\delta-E(k'')}. \tag{3.5}$$

The details of the calculation of the partial wave com-

ponents $\hat{U}_{LJ}$ of the optical potential in terms of the microscopic ingredients ($t$ matrix and density) is provided in the Appendix. We summarize here the important formulae in two steps. In terms of the partial wave components of the quantities $\hat{U}^c(\vec{k}',\vec{k})$ and $\hat{U}^{LS}(\vec{k}',\vec{k})$, we have

$$\hat{U}_{LJ}(k',k)=\hat{U}^c_L(k',k)+C_{LJ}\hat{V}^{LS}_L(k',k)\ , \tag{3.6}$$

where

$$C_{LJ}=\tfrac{1}{2}[J(J+1)-L(L+1)-\tfrac{3}{4}] \tag{3.7}$$

and

$$\hat{V}^{LS}_L(k',k)=-\frac{k'k}{2L+1}[\hat{U}^{LS}_{L-1}(k',k)-\hat{U}^{LS}_{L+1}(k',k)]\ . \tag{3.8}$$

To obtain these results, the quantities $\hat{U}^c(\vec{k}',\vec{k})$ and $\hat{U}^{LS}(\vec{k}',\vec{k})$ are expanded in a manner similar to Eq. (3.2) with the exception that the partial wave components ($\hat{U}^c_L$ and $\hat{U}^{LS}_L$) are independent of $J$. If the position-space representations of $\hat{U}^c(\vec{k}',\vec{k})$ and $\hat{U}^{LS}(\vec{k}',\vec{k})$ were purely local functions of the projectile-nucleus relative separation [say $\hat{U}^c(\vec{r})$ and $\hat{U}^{LS}(\vec{r})$], then the results of Eqs. (3.6)–(3.8) are equivalent to the representation

$$\hat{U}(\vec{r})=\hat{U}^c(\vec{r})+\hat{V}^{LS}(\vec{r})\vec{L}\cdot\vec{S}\ , \tag{3.9}$$

where

$$\vec{L}=\vec{r}\times\frac{1}{i}\vec{\nabla}_r,\quad \vec{S}=\tfrac{1}{2}\vec{\sigma}\ ,$$

and

$$\hat{V}^{LS}(\vec{r})=\frac{1}{r}\frac{d}{dr}\hat{U}^{LS}(\vec{r})\ . \tag{3.10}$$

The microscopic content of $\hat{U}^c$ and $\hat{U}^{LS}$, given in Eqs. (2.34) and (2.35) for optimum factorization, does not lead to local forms, and thus microscopically based departures from the simple (standard) forms [Eqs. (3.9) and (3.10)] for optical potentials are included in the optimum factorization calculations.

The partial wave components of $\hat{U}^c(\vec{k}',\vec{k})$ and $\hat{U}^{LS}(\vec{k}',\vec{k})$ can be calculated in terms of NN $t$-matrix components and nuclear densities from Eqs. (2.34) and (2.35). For example, the projection can be performed numerically by evaluating the integral

$$\hat{U}^c_L(k',k)=\tfrac{1}{2}\int_{-1}^{+1}dx\,P_L(x)\hat{U}^c(\vec{k}',\vec{k})\ , \tag{3.11}$$

$$=\tfrac{1}{2}\int_{-1}^{+1}dx\,P_L(x)\frac{A-1}{A}\eta\sum_{\alpha=\mathrm{n,p}}t^c_\alpha\left[\epsilon;\vec{q}(x),\frac{A+1}{A}\vec{K}(x)\right]\rho^\alpha[q(x)]\ , \tag{3.12}$$

where $q^2(x)=k'^2+k^2-2k'kx$, $K^2(x)=\frac{1}{4}(k'^2+k^2+2k'kx)$, and $\vec{q}\cdot\vec{K}=\frac{1}{2}(k'^2-k^2)$. Alternatively, in terms of partial wave components of $t^c_\alpha$, $t^{LS}_\alpha$, and $\rho^\alpha$ defined with the same convention as Eq. (3.11), the result can be expressed as

$$U^c_L(k',k)=\frac{A-1}{A}\eta\sum_{l,l'}\sum_{\alpha=\mathrm{n,p}}\beta_{l,l',L}t^c_{\alpha,l}(k',k)\rho^\alpha_{l'}(k',k)\ , \tag{3.13}$$

where

$$\beta_{l,l'L}=\frac{(2l+1)(2l'+1)}{2L+1}\langle l0;l'0\,|\,L0\rangle^2\ . \tag{3.14}$$

For both methods, analogous results hold for $\hat{U}^{LS}_L(k',k)$. We have employed both methods as a check on the accuracy of the numerical procedures.

The one-dimensional integral equation [Eq. (3.5)] for the partial wave elements $\hat{T}_{LJ}$ is treated by separating the principal value and on-shell delta-function components of the propagator. Thus, Eq. (3.5) becomes a pair of equations, namely the $K$-matrix Lippmann-Schwinger equation,

$$\hat{R}_{LJ}(k',k)=\hat{U}_{LJ}(k',k)+4\pi\mathrm{P}\int_0^\infty k''^2dk''\frac{\hat{U}_{LJ}(k',k'')\hat{R}_{LJ}(k'',k)}{E(k)-E(k'')}\ , \tag{3.15}$$

and the Heitler equation,

$$\hat{T}_{LJ}(k',k)=\hat{R}_{LJ}(k',k)-i\lambda k\hat{R}_{LJ}(k',k)\hat{T}_{LJ}(k,k)\ , \tag{3.16}$$

where

$$\lambda=(2\pi)^2\frac{E_\mathrm{N}(k)E_A(k)}{E_\mathrm{N}(k)+E_A(k)}\ . \tag{3.17}$$

Here, $k$ is the on-shell momentum in units of MeV/$c$ and $E(p)=E_\mathrm{N}(p)+E_A(p)$ where the energies are given by $E^2_\mathrm{N}(p)=p^2+m^2_\mathrm{N}$ for the projectile and $E^2_A(p)=p^2+m^2_A$ for the target. We have used

$$\lim_{\epsilon\to0}(x+i\epsilon)^{-1}\equiv P\left[\frac{1}{x}\right]-i\pi\delta(x)$$

with

$$\delta[E(k)-E(k'')]=\frac{\lambda}{(2\pi)^2k}\delta(k-k'')\ . \tag{3.18}$$

After Eq. (3.15) is solved for $\hat{R}_{LJ}$, the Heitler unitarity equation (3.16) gives the on-shell $\hat{T}_{LJ}$ as an algebraic expression. This unitarity constraint ensures that the on-shell $\hat{T}_{LJ}$ has the form

$$\hat{T}_{LJ}(k,k)=-\frac{1}{\lambda}\frac{e^{2i\delta_{LJ}}-1}{2ik}\ , \tag{3.19}$$

where $\delta_{LJ}$ is a real phase shift if $\hat{U}_{LJ}$ and, hence, $\hat{R}_{LJ}$ are real. The corresponding physical scattering amplitude (in units of fm) is given by

$$F_{LJ}=-\hbar c\frac{A}{A-1}\lambda\hat{T}_{LJ}(k,k)\ , \tag{3.20}$$

where the scaling factor $A/A-1$, required by the KMT procedure, is included. The full scattering amplitude, as an operator in spin space, is then obtained in the standard fashion as

$$F(\theta)=A(\theta)+i\vec{\sigma}\cdot\hat{n}C(\theta)\ , \tag{3.21}$$

where

$$A(\theta)=\sum_{L=0}^{\infty}[(L+1)F_L^+ +LF_L^-]P_L(\cos\theta) \tag{3.22}$$

and

$$C(\theta)=\sum_{L=1}^{\infty}(F_L^+ -F_L^-)P_L^1(\cos\theta)\ . \tag{3.23}$$

Here $\hat{n}$ is the unit vector in the direction $\vec{k}'\times\vec{k}$, where $\vec{k}'$ is the final momentum, and $F_L^{\pm}$ denotes $F_{LJ}$ for $J=L\pm\frac{1}{2}$, respectively.

### B. Treatment of the Coulomb potential

There are essentially two problems associated with the inclusion of the Coulomb interaction of the projectile with the charge density of the nucleus into KMT optical potential calculations for elastic scattering of the type considered here. The lesser of the two problems concerns the question of whether the KMT scaling factor of $A-1/A$ should multiply both the nuclear and Coulomb parts of the optical potential. When Coulomb excitation of the nucleus is ignored, as it always is compared to the strong nuclear excitation, the correct procedure is to add the Coulomb potential for the interaction of the projectile with the distributed charge of the nucleus to the physical (Watson) nuclear optical potential [Eq. (2.5)]. The procedures presented following Eq. (2.5) for the replacement of the inconvenient nuclear NN operator $\tau$ by the more convenient nuclear NN operator $t$ introduces the $A-1/A$ scaling of only the short range nuclear contributions to the KMT nucleon-nucleus transition operator $\hat{T}$. This topic has been discussed previously.[20] In summary the required KMT first-order optical potential is given by

$$U'(\vec{k}',\vec{k})=\left\langle\vec{k}',\phi_0\left|\sum_{i=1}^{Z}v_{0i}^c\right|\phi_0,\vec{k}\right\rangle + \frac{A-1}{A}\left\langle\vec{k}',\phi_0\left|\sum_{i=1}^{A}t_{0i}\right|\phi_0,\vec{k}\right\rangle\ , \tag{3.24}$$

$$=V^c(q)+\hat{U}(\vec{k}',k)\ , \tag{3.25}$$

where $\hat{U}$ is the nuclear potential we have already discussed, $V^c(q)$ is the distributed Coulomb potential given by $v^c(q)\rho_{ch}(q)$, where $v^c(q)$ is the momentum-space Coulomb potential between the projectile and a proton. The required procedure is to calculate only the Coulomb-distorted (nuclear-bar) scattering amplitude from $U'$, to apply the factor $A/A-1$ to obtain the physical nuclear-bar scattering amplitude, and then to add the Coulomb scattering amplitude due to $V^c(q)$. This standard procedure is simple to implement when the approach of a wave equation in position space is followed.

However, for a momentum-space integral equation approach the equivalent of this procedure is not straightforward. This is the second problem that is alluded to above. A direct calculation of the nuclear-bar transition amplitude via an integral equation involves Coulomb distorted Green's functions in momentum space. The method proposed by Vincent and Phatak[21] avoids this problem and is a practical procedure which is exact, in principle. Its accuracy has been documented for low angular momentum states and low momentum transfers that are typical of low energy pion scattering from nuclei. We find that the method is numerically unstable and not reliable in its present form for the high angular momentum states and larger momentum transfers typical of intermediate energy proton scattering from nuclei. Let us consider the position space Coulomb potential separation

$$V^c(r)=V_1^c(r)+V_2^c(r)\ ,$$

where

$$V_1^c(r)=V^c(r)\theta(R-r)$$

and

$$V_2^c(r)=V^c(r)\theta(r-R)\ .$$

Here $R$ is a radius outside of which the nuclear potential is negligible. In momentum space, only the exterior potential $V_2^c(q)$ has the $1/q^2$ singularity. The Vincent-Phatak method consists of solving the Lippmann-Schwinger equation with the potential $V_1^c(q)+\hat{U}(k',k)$ to obtain phase shifts $\delta'_{LJ}$ from which the corresponding position-space radial wave function at the point $R$ can be constructed. This wave function is then to be matched to the usual sum of regular and irregular pure Coulomb radial wave functions at the point $R$ to obtain the desired nuclear-bar phase shifts $\bar{\delta}_{LJ}$. This momentum-space procedure would accurately reproduce the (exact) position-space results if $V_1^c(q)$ could be treated accurately in solving the Lippmann-Schwinger equation. However, $V_1^c(q)$ involves the Fourier transform of a straight edge cutoff and the required partial wave components $V_{1,L}^c(k',k)$ will in practice contain spurious contributions, especially for high angular momentum states. Since $V_1^c$ and $V_2^c$ are treated numerically in different ways it is difficult to avoid spurious sharp edge diffractive oscillations in computed observables at high momentum transfer. The convergence of partial wave expansions is easily lost.

The method that we employ involves the separation

$$V^c(q)=V_{pt}^c(q)+V_s^c(q)\ , \tag{3.26}$$

where $V_{pt}^c(q)$ is the Coulomb potential due to a point charge $Ze$, and $V_s^c(q)$ is the remainder, which is of short range. From Eq. (3.25) the total first-order optical potential is written as

$$U'(\vec{k}',\vec{k})=V_{pt}^c(q)+\hat{U}'(\vec{k}',\vec{k})\ , \tag{3.27}$$

where the total short-range piece is

$$\hat{U}'(\vec{k}',\vec{k})=V_s^c(q)+\hat{U}(\vec{k}',\vec{k}) . \tag{3.28}$$

The total scattering amplitude due to the potential $U'(\vec{k}',\vec{k})$ can be written in the standard way as

$$F(\theta)=A(\theta)+i\vec{\sigma}\cdot\hat{n}C(\theta) , \tag{3.29}$$

where now instead of Eqs. (3.22) and (3.23) we have

$$A(\theta)=F_{pt}^c(\theta)+\sum_{L=0}^{\infty} e^{2i\sigma_L}[(L+1)\bar{F}_L^+ +L\bar{F}_L^-] \times P_L(\cos\theta) \tag{3.30}$$

and

$$C(\theta)=\sum_{L=1}^{\infty} e^{2i\sigma_L}(\bar{F}_L^+ -\bar{F}_L^-)P_L^1(\cos\theta) . \tag{3.31}$$

Here $F_{pt}^c(\theta)$ is the Rutherford amplitude for Coulomb scattering from a point charge, $\sigma_L$ is the corresponding Coulomb phase shift, and $\bar{F}_L^{\pm}$ are the nuclear-bar scattering amplitudes due to $\hat{U}'(\vec{k}',\vec{k})$. That is, the distortion effects due to $V_{pt}^c(q)$ are included in $\bar{F}_L^{\pm}$. Since the major part of the Coulomb-nuclear interference effect is carried out by the interference of the two terms in Eq. (3.30) and the presence of the $e^{2i\sigma_L}$ factors in Eqs. (3.30) and (3.31), and since the nuclear-bar amplitudes are quite close to the pure short-range amplitudes, we replace $\bar{F}_L^{\pm}$ by scattering amplitudes due to the short-range potential $\hat{U}'(\vec{k}',\vec{k})$ only. We found this approximation to be more useful over the large range of momentum transfers and angular momenta involved than the method based on dealing with the cutoff $\theta(R-r)$ translated to momentum space.

### C. Treatment of high angular momentum states

For proton scattering at intermediate energies the number of $L$ values needed to represent the nuclear optical potential $\hat{U}(\vec{k}',\vec{k})$ at the level of accuracy we require through the partial-wave components $\hat{U}_{LJ}(k',k)$ can be as large as 60 for a $^{40}$Ca target at 500 MeV and 120 for a $^{208}$Pb target at 800 MeV. The procedures expressed by Eq. (3.12) or Eq. (3.13) for calculating $U_{LJ}(k',k)$ become increasingly difficult to perform accurately for high values of $L$. This problem can be alleviated through the use of the three-dimensional Born approximation to the scattering amplitude to account for the infinite set of $L$ values satisfying the condition $L>L_c$, where $L_c$ is such that the Born approximation is sufficiently accurate. That is, Eqs. (3.30) and (3.31) are evaluated in the forms

$$A(\theta)=F_{pt}^c(\theta)+\sum_{L=0}^{L_c} e^{2i\sigma_L}[(L+1)\bar{F}_L^+ +L\bar{F}_L^-]P_L(\cos\theta) +e^{2i\sigma_{L_c+1}}A_B^>(\theta) \tag{3.32}$$

and

$$C(\theta)=\sum_{L=1}^{L_c} e^{2i\sigma_L}(\bar{F}_L^+ -\bar{F}_L^-)P_L^1(\cos\theta)+e^{2i\sigma_{L_c+1}}C_B^>(\theta) , \tag{3.33}$$

where

$$A_B^>(\theta)=A_B(\theta)-\sum_{L=0}^{L_c}[(L+1)F_{B,L}^+ +LF_{B,L}^-]P_L(\cos\theta) \tag{3.34}$$

and

$$C_B^>(\theta)=C_B(\theta)-\sum_{L=1}^{L_c}(F_{B,L}^+ -F_{B,l}^-)P_L^1(\cos\theta) . \tag{3.35}$$

Here $A_B(\theta)$ and $C_B(\theta)$ are the scattering amplitudes due to the short range potential $\hat{U}'(\vec{k}',\vec{k})$ in the Born approximation, determined without angular momentum projection, and $F_{B,L}^{\pm}$ are the corresponding partial-wave projections for low angular momenta. Since the angular momentum components of $A_B^>(\theta)$ and $C_B^>(\theta)$ are not separated, it is not possible to properly include in Eqs. (3.32) and (3.33) the Coulomb distortion factors $e^{2i\sigma_L}$ for each $L>L_c$. Since $\sigma_L$ is slowly varying with $L$ for large $L$, we have adopted the procedure of multiplying by the single factor $e^{2i\sigma_{L_c+1}}$. The Born amplitudes in three-dimensional form $A_B^>(\theta)$ and $C_B^>(\theta)$ are calculated directly from the short range optical potential $\hat{U}'(k',k)$ given by Eqs. (3.28), (2.33), (2.34), and (2.35) by removing the KMT scaling factors $A-1/A$, applying the on-shell condition $|\vec{k}'|=|\vec{k}|$, and multiplying by $-\hbar c\lambda$ to produce the properly normalized scattering amplitude in units of fm. This procedure, represented by Eqs. (3.32)—(3.35), essentially includes an infinite number of partial waves.

## IV. RESULTS

### A. Off-shell and nonlocal effects

In Figs. 2 and 3 the scattering observables calculated from the various factorization treatments of the first order optical potential are compared with each other and also with data for elastic proton scattering from $^{40}$Ca at 500 MeV. The point proton density was obtained from the nuclear charge density which was taken to be a three-parameter Fermi shape with the parameters fixed at the values determined by an analysis of electron scattering data.[23] The point neutron density was set equal to the point proton density. This same procedure was followed in all calculations used to explore the influence of off-shell and nonlocal effects as described in this section. It is obvious from the differential cross section calculations shown in Fig. 2 that with small adjustments of the density parameters (especially those for the neutrons) a much improved agreement with the data could be achieved. However, the object of the present investigation is to test the sensitivity to the manner in which off-shell and nonlocal effects are treated in the implementation of the first-order theory of the optical potential.

The solid curve results from the optimum factorization [Eqs. (2.33)—(2.35)] procedure in which the optical potential is nonlocal and includes off-shell elements of the NN $t$ matrix. The energy of the NN $t$ matrix is fixed at the

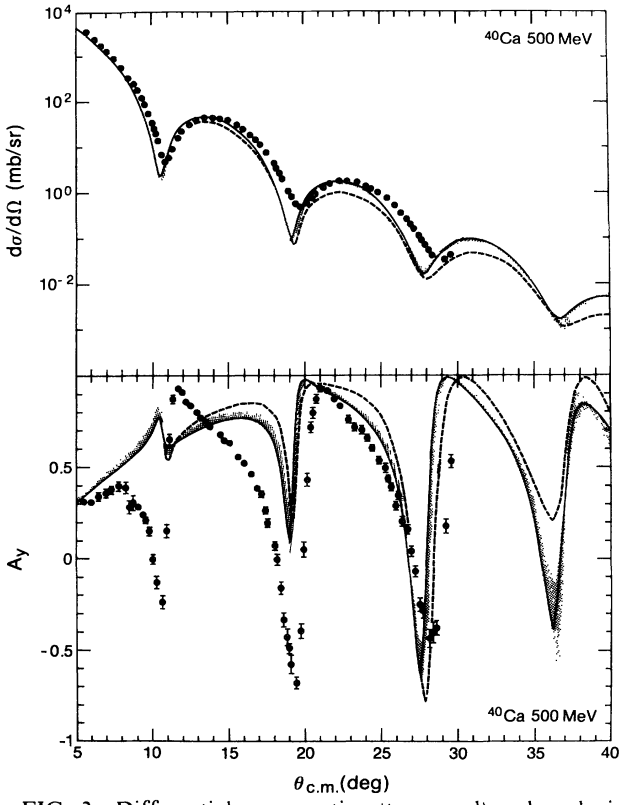


FIG. 2. Differential cross section (top panel) and analyzing power (bottom panel) for protons scattered from $^{40}$Ca at 500 MeV, calculated with the first-order (KMT) optical potential. The solid curve represents the optimum factorization calculation which incorporates off-shell and nonlocal effects, the dashed curve represents the usual on-shell factorization procedure. The shaded band displays an estimate of the range of uncertainties to be expected from approximate treatments of the folding integral. The data are from Ref. 22.

value corresponding to NN scattering at the beam energy. The dashed curve represents the results from the OS1 prescription [Eqs. (2.38) and (2.39)] which is the on-shell factorization procedure that is almost invariably employed in representations of first order optical potentials.

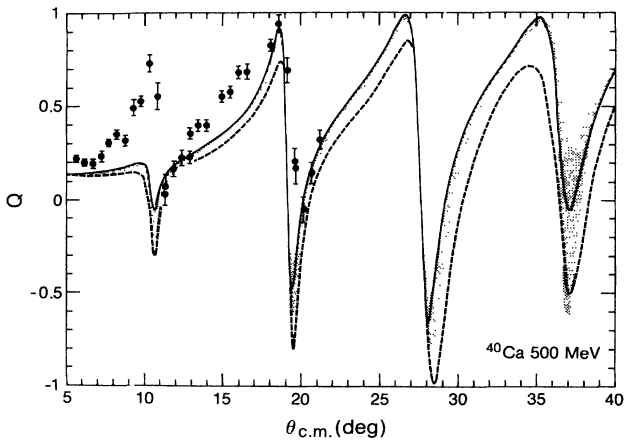


FIG. 3. The spin rotation function $Q$ for protons scattered from $^{40}$Ca at 500 MeV with everything else as in Fig. 2. The data are from Ref. 31.

The energy of the NN $t$ matrix is again fixed as described previously. The corresponding optical potential is local and contains no off-shell NN information whatsoever. The qualitative features of both these calculations are the same for the angular range shown. However, if details of the nuclear densities were varied to fit data, different densities would be deduced from the two prescriptions. In the first Born approximation, the OS1 prescription gives no scattering beyond about 60°, because, as described in Sec. III, this is the limit of the on-shell region for NN scattering at the beam energy. A part of the difference between the solid and dashed curves, particularly beyond 20°, is attributable to this cutoff introduced by the nature of the on-shell factorization procedure. The only information we infer from the difference between the solid and dashed curves is that, with a fixed energy of the NN $t$ matrix, a model of the off-shell behavior is needed for accurate quantitative analysis of data. At 500 MeV this effect is, nevertheless, small compared to other effects that have not been included with calculations shown here. We will return to this point shortly.

The shaded regions in Figs. 2 and 3 are an estimate of the uncertainty we introduce by using a factorization method instead of performing the full-folding integral for the first-order optical potential. The variations away from the optimum factorization result introduced by the asymptotic momentum (ASM) approximation and the variable NN energy on-shell factorized prescription (OS2) have been used to define the shaded regions. In both these latter cases the optical potential is local. For the ASM, off-shell elements of the NN $t$ matrix enter at a fixed NN energy, while for the OS2, the $t$ matrix is on shell but the effective NN energy is defined by the invariant NN mass which introduces a coupling to the kinematics of the reaction process as described in Sec. II. Consequently, the shaded regions may be viewed as also yielding an indication of the typical size of off-shell and nonlocal effects. The main point to be made for 500 MeV is that off-shell and nonlocal effects, and the way these aspects are handled in treatments of the full-folding integral, do not lead to a significant change in the qualitative nature of the scattering observables. This is due in large part to the limited angular range over which interest can be focused because of the rapid falloff of the cross sections. At lower energies and for lighter targets, the off-shell and nonlocal effects can be significant in regions where data exists.

At 500 MeV the discrepancy between any of the theoretical calculations shown here and the experimental data is of more significance than differences between the individual calculations. Relativistic effects that can be incorporated through the use of a Dirac equation together with a microscopically based ansatz for the first-order optical potential transformed to the appropriate spinor basis have been shown to be much more sizable.[9] In the particular case of $^{40}$Ca at 500 MeV, such relativistic calculations with the same density parameters employed here improve the description of the experimental cross section by causing the diffraction minima to be shallower and shifted to larger angles, in agreement with the data. More dramatic improvements are likewise obtained for the analyzing power and spin rotation functions for all angles

where data are available, especially at $\sim 10°$ where $A_y$ and $Q$ have the wrong qualitative behavior in nonrelativistic treatments. However, the off-shell and nonlocal effects studied here for the nonrelativistic treatment have their analogs in the relativistic treatment, and one would expect a comparable amount of uncertainty from these sources in the latter case. This is indeed the case as will be discussed in a further publication.[24] Thus accurate quantitative analysis of data require not only the incorporation of purely relativistic features but also nonlocal and off-shell effects, as well as an understanding of the importance of any medium-dependent departure from the free NN $t$ matrix and higher-order scattering mechanisms.

We show in Figs. 4 and 5 the corresponding results for $^{40}$Ca at a beam energy of 181 MeV. The dashed line, which represents the fixed energy on-shell factorization prescription OS1, is terminated at $\sim 60°$. The reason for this is that the OS1 prescription involves a sharp cutoff in the optical potential at this point which gives rise to unphysical behavior in the angular distribution just beyond $\sim 60°$. After about 15°—20° beyond this point the dashed curve lies close to, or within, the shaded band. This evidently occurs because the amplitude for large angle scattering is dominated by multiple small angle scattering. Such behavior is typical of OS1 in the other cases discussed below. The off-shell and nonlocal effects represented by the shaded regions become more sizable as the scattering angle is increased. The structure of the analyzing power as a function of angle at this energy only roughly resembles the experimental data.[25] The minima are too shallow and they occur at too small angles at this energy. The first order truncation of the multiple scattering expansion for the optical potential is questionable as is the use of a free NN $t$ matrix.

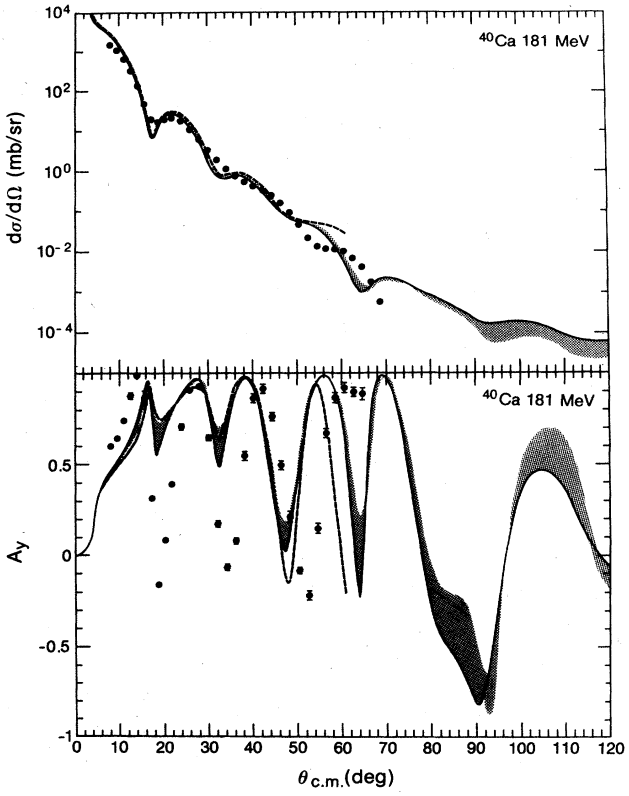


FIG. 4. Same as Fig. 2 except that the proton energy is 181 MeV and the data are from Ref. 25.

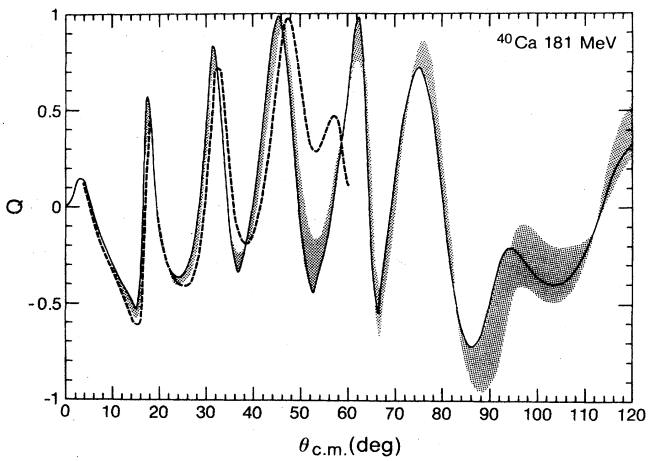


FIG. 5. Same as Fig. 3 except that the proton energy is 181 MeV.

Approximate treatments of the nuclear density dependence of the effective NN scattering operator introduced by Pauli exclusion effects have been seen in the case of 135 MeV scattering from $^{16}$O to deepen the minima in analyzing power calculations.[26] Relativistic extensions employing the same ansatz as has been successful for 500 MeV also produce deep minima in the 181 MeV analyzing power, but the effect appears much too strong and the resulting differential cross section is shifted significantly away from the data compared to the nonrelativistic result shown here.[27] At this energy it seems likely that a comprehensive theoretical approach, combining nuclear medium effects on the NN $t$ matrix together with a better microscopic understanding of the appropriate relativistic extension of first-order theory, may provide a much improved description. Off-shell and nonlocal effects (among others) need to be addressed for accurate calculations of spin-dependent scattering observables.

The situation for a light target is displayed in Figs. 6 and 7 for $^{16}$O at 318 MeV, and in Fig. 8 for $^{16}$O at 135 MeV. As is evident from the shaded regions, there is relatively little sensitivity to off-shell and nonlocal effects at 318 MeV. This is most likely due to the weak strength of the spin-independent part of the NN $t$ matrix which arises from the near cancellation of the effects of short range repulsion and long range attraction in this energy regime. However, as seen from Fig. 8, these effects become quite significant at energies near 100 MeV, especially for spin-dependent observables. The extent of the agreement with data for the cross section resulting from the optimum factorization treatment of the first-order optical potential is somewhat surprising for an energy as low as 135 MeV. This result raises the expectation that a first-order theory of the optical potential supplemented with the essential physical features of additional processes not considered here (medium effects, antisymmetrization effects, and rel-

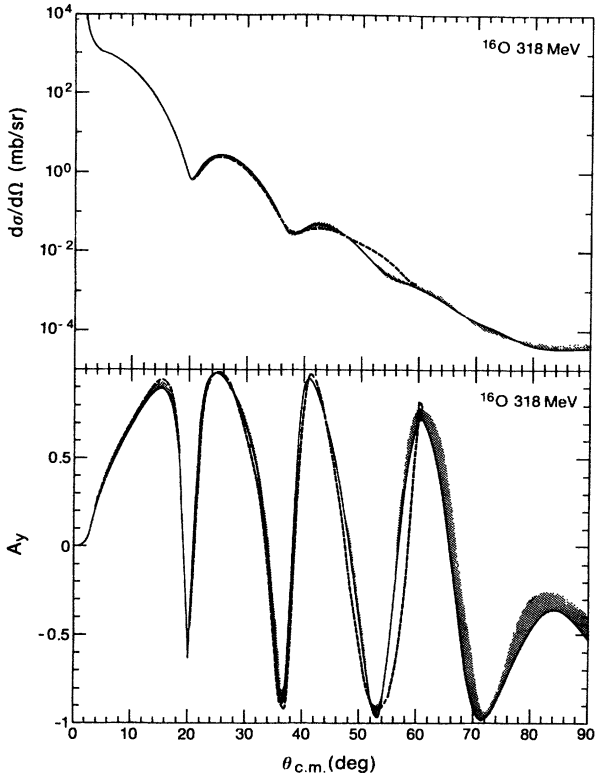


FIG. 6. Same as Fig. 2 except for $^{16}$O at 318 MeV.

ativistic extensions), but still within the general mold of a first-order scattering mechanism, may lead to a reasonably accurate description of the relatively small interference mechanisms that are focused upon in analyzing power measurements. The shaded regions in Fig. 8 indicate that, in such a task, the off-shell and nonlocal features of the first-order theory must be addressed in order for the results to be theoretically reliable. Put another way, it is clear from our work that there is considerable sensitivity near 100 MeV to how the so-called full-folding integral [Eq. (2.26)] for the first-order optical potential is handled. The size of the shaded band in Fig. 8 suggests that nothing less than an accurate evaluation of this in-

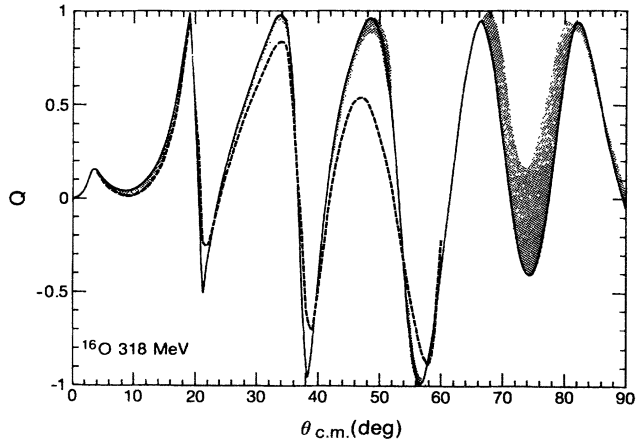


FIG. 7. Same as Fig. 3 except for $^{16}$O at 318 MeV.

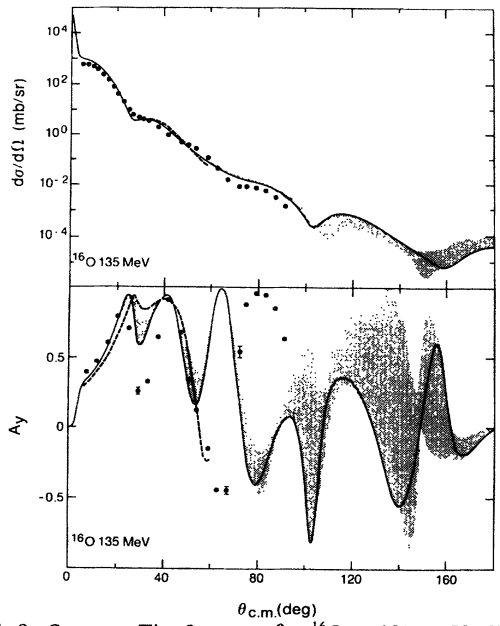


FIG. 8. Same as Fig. 2 except for $^{16}$O at 135 MeV. The data are from Ref. 26.

tegral (rather than factorization procedures) can be used to represent the first-order term of the optical potential. This suggestion remains just as relevant in cases where medium modifications are included in the NN scattering operator and where higher order mechanisms in the optical potential are to be included. An important consideration for these lower energies and light targets is that the momentum changes supported by the nuclear density matrix and the NN scattering operator are more nearly equal than is the case at laboratory energies of several hundred MeV and for heavy targets.

### B. Uncertainties in the nuclear densities

In Figs. 9—16 we show the results of calculations in which the nuclear densities are taken from different sources. For these figures, only the optimum factorization prescription for the optical potential has been employed. In each figure the solid curve corresponds to the solid curves shown in the earlier figures. That is, the point neutron density was set equal to the point proton density, which in turn was obtained from the nuclear charge density. The latter was described as a three-parameter Fermi shape with the parameters taken from a compilation[23] of electron scattering analyses. The variations away from this solid curve result obtained by employing two other sources of nuclear densities are shown as a shaded band. These two alternative sources of nuclear density information are (1) a shell model calculation[28] using Woods-Saxon single particle potentials with the various parameters constrained by energy levels, transition rates, and electron scattering information, and (2) fits[29] to electron scattering form factors in terms of a three-parameter Fermi shape supplemented by other functions to improve the description of the data at high momentum transfer. In the shell model case, the point

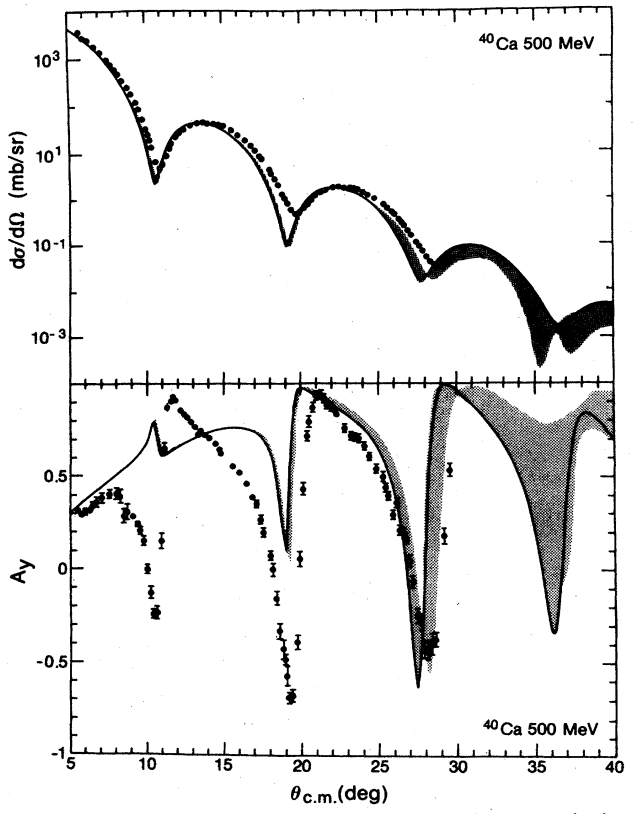


FIG. 9. Differential cross section (top panel) and analyzing power (bottom panel) for protons scattered from $^{40}$Ca at 500 MeV, calculated with the optimum factorization prescription. The shaded band represents the uncertainty in the physical observable due to the uncertainty in the nuclear density. The data are from Ref. 22.

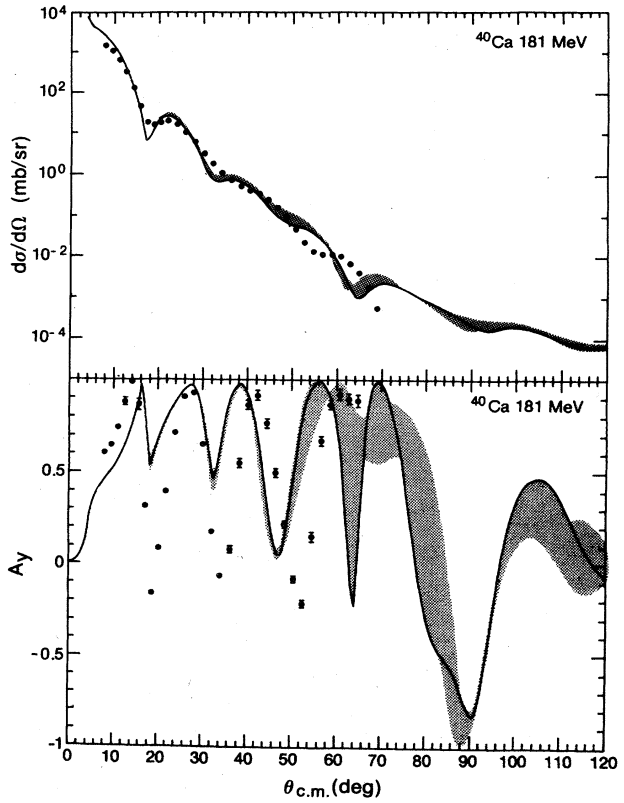


FIG. 11. Same as Fig. 9 except for $^{40}$Ca at 181 MeV. The data are from Ref. 25.

neutron and proton densities are not identical, while in the second case the point neutron density is taken to be identical to the point proton density.

As one would expect, these differing descriptions of the nuclear densities have essentially no effect on the calculated scattering observables for very forward angles throughout the energy range 100—500 MeV. However, the model dependence of the nuclear density introduces uncertainties in the scattering observables which increase significantly with increasing momentum transfer, as can be seen by comparing the shaded bands in Figs. 9—16 with those in Figs. 2—8. We have checked the fact that in the large momentum transfer regions of our calculations, ambiguities in how the electron scattering based densities should be extrapolated beyond the regions constrained by the data do not give results outside the shaded bands shown. The influence of the density uncertainties are comparable to, and often greater than, the influence of

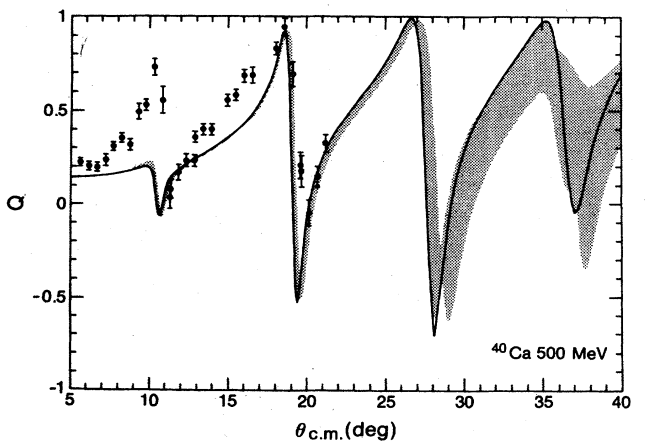


FIG. 10. Spin rotation function $Q$ for $^{40}$Ca at 500 MeV, otherwise as in Fig. 9. The data are from Ref. 31.

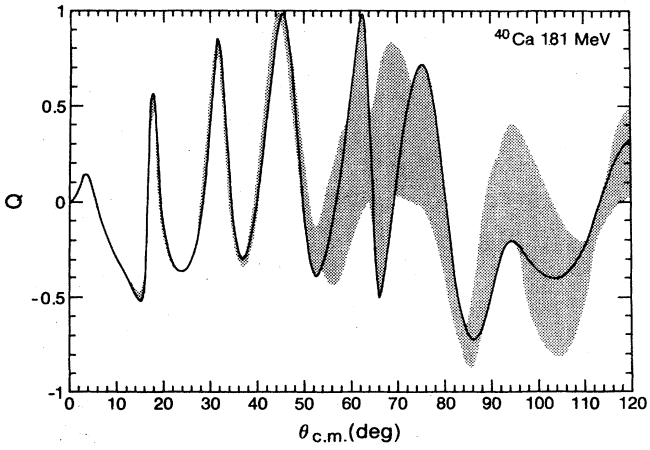


FIG. 12. Same as Fig. 10 except for $^{40}$Ca at 181 MeV.

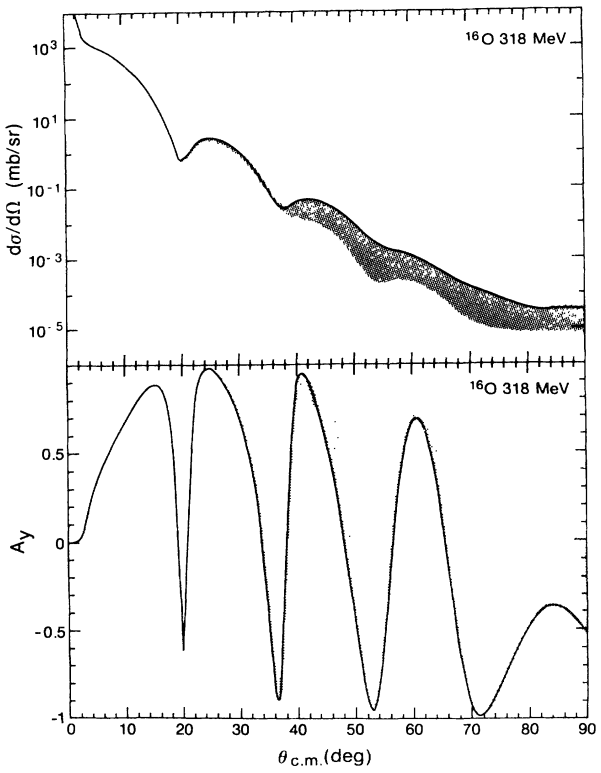


FIG. 13. Same as Fig. 9 except for $^{16}$O at 318 MeV.

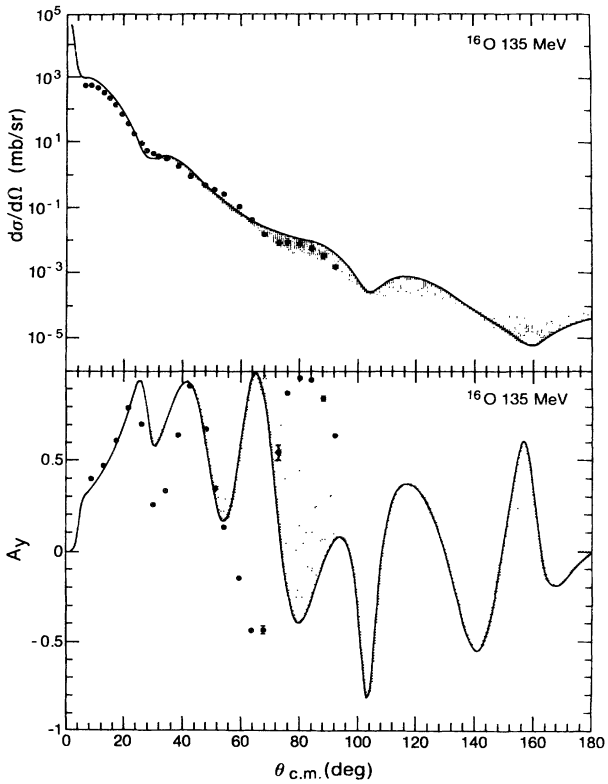


FIG. 15. Same as Fig. 9 except for $^{16}$O at 135 MeV. The data are from Ref. 26.

uncertainties due to off-shell and nonlocal effects. For example, for scattering on $^{40}$Ca at 500 MeV, the density ambiguities for scattering angles beyond about 25° are significantly larger than the ambiguities due to off-shell and nonlocal effects. The same situation holds for $^{16}$O at 318 MeV for scattering angles beyond about 35°. Extraction of density information by fitting data at such energies would seem to be a valid exercise so long as little importance is attached to distinguishing fits which lie inside the "envelope of uncertainty" due to off-shell and nonlocal effects. To go further than that requires reliable input for the off-shell and nonlocal structure of the NN scattering operators and the elimination or accurate justification of the factorization representation of the full-folding integral.

For the lower energy cases of $^{40}$Ca at 181 MeV and $^{16}$O at 135 MeV the ambiguities due to densities and off-shell—nonlocal effects are comparable, with the latter extending to lower scattering angles. This finding, together with the strong likelihood that higher order mechanisms for the optical potential are also important for these energies, reinforces the need to develop accurate methods for calculation of the first-order mechanism. In this regard, a realistic model for the off-shell matrix elements of the NN scattering operator should also be employed. The

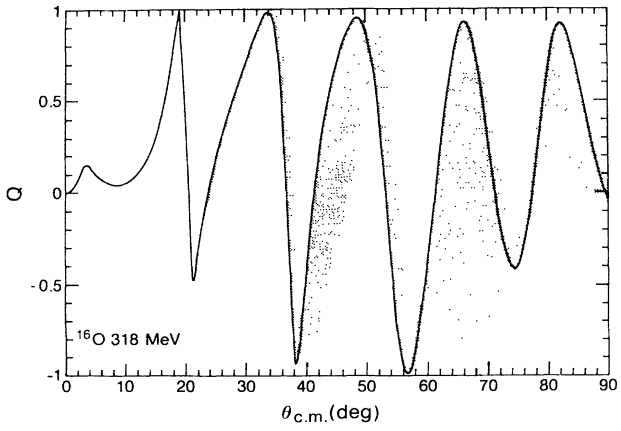


FIG. 14. Same as Fig. 10 except for $^{16}$O at 318 MeV.

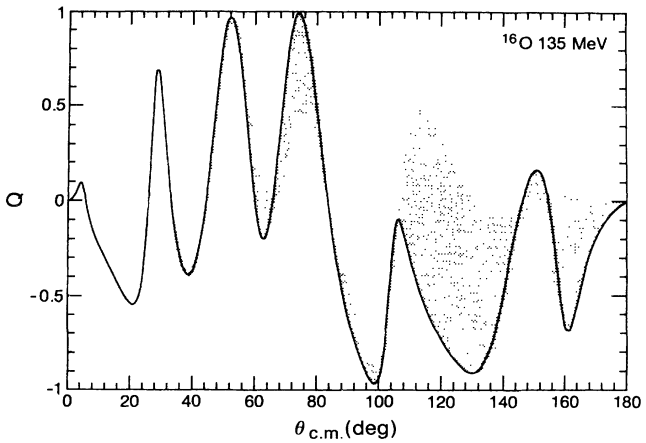


FIG. 16. Same as Fig. 10 except for $^{16}$O at 135 MeV.

Love-Franey model of $t_{NN}$ that we have employed only contains off-shell and nonlocal effects that can be manifested through the interplay of a direct and exchange term each of which is obtained from an intrinsically local function. Work is in progress on the construction of optical potentials from a $t_{NN}$ generated from realistic NN potential models.[30]

## V. SUMMARY AND CONCLUSIONS

In the preceding text we have described in some detail the nonrelativistic momentum-space proton-nucleus calculations we have performed for and with the first-order KMT type of optical potential. The calculations presented are designed to yield a picture of the reliability and the range of variability of predictions based upon the first-order optical potential due to uncertainties in the input quantities. The basic input quantities in the calculations are the on-shell two-body $t$ matrix, its nonlocal character and off-shell extension, the treatment of the full-folding integral, and nuclear densities taken from electron scattering. Comparison of calculations using the Love-Franey $t$ matrix as opposed to direct use of the phase shifts indicates the on-shell $t$ matrix is under very good control.[3] Energy and momentum transfer regimes of sensitivity and insensitivity to off-shell and nonlocal effects and to the treatment of the folding integral have been indicated. Work is currently in progress[30] which will yield further information and documentation relative to these sensitivities by removing the particular locality and nonlocality assumption implicit in the Love-Franey parametrization. However, it is presently clear that in order to analyze data confidently below $\sim 200$ MeV, and at large scattering angles, both the $t$ matrix and the folding integral must be precisely treated. On the other hand, the regimes of sensitivity to the nuclear density are not of precisely the same character. Comparison of the figures indicates regimes where density sensitivities are much greater than for the other sources of uncertainty studied in this paper so that density information may be extracted. Of course other sources of uncertainty, not studied herein, certainly bear on this issue. Nevertheless, these sources of ambiguity are in addition to the ones we have investigated and the current work represents the best (only) detailed study to date of the reliability of predictions made on the basis of the first-order optical potential.

From this study we may conclude that the anomaly in the spin observables for $^{40}$Ca at 500 MeV, for example, represents a true failure of the first order KMT type of optical potential to give a complete description of the data. The recent successful work with the Dirac equation,[9] in which the effect of virtual pair production and annihilation is added to the nonrelativistic multiple scattering theory, is thus more firmly founded than in the absence of these studies. It must be emphasized, however, that other effects not included in the nonrelativistic first-order multiple scattering approach used here may need to be taken into account and that this is by no means excluded by the present study. At any rate, these effects must be investigated to the point where they are under reliable control, both theoretically and computationally.

Subject to the limitations mentioned already, the sensitivity to off-shell and nonlocal effects, as well as to treatments of the full-folding integral, has been documented in this work. We find that for small and moderate momentum transfer at high energies the standard approximations are tenable. We further conclude that systematic study of data at higher momentum transfer will yield physically interesting information, provided a reliable theoretical framework and careful calculations are employed.

These assertions follow not only from the representative results explicitly shown herein, but also from a large number of additional calculations performed for other targets and energies, as well as from other variations of the input assumptions.

## ACKNOWLEDGMENTS

The authors are grateful for the support provided by the Los Alamos National Laboratory in all phases of this work. Particular thanks are due to M. V. Hynes, whose knowledge of the experimental situation both for electron and nucleon scattering proved invaluable. We wish to acknowledge D. J. Ernst, L. Ray, and F. Tabakin for useful discussions. Partial support was provided by the U.S. Department of Energy under Grant No. DE-AS05-76-ER05126, and the National Science Foundation under Grants No. PHY-83-05745, No. PHY-79-07511, and No. PHY-81-21956.

## APPENDIX: ANGULAR MOMENTUM PROJECTIONS

The details of the derivation of the results given in Eqs. (3.6)—(3.8) for the angular momentum projections of the nuclear part of the optical potential of Eq. (3.1) are outlined here. We begin with Eq. (3.1) in the form

$$\hat{U}(\vec{k}',\vec{k})=\hat{U}^{c}(\vec{k}',\vec{k})+\frac{i}{2}\vec{\sigma}\cdot\vec{k}'\times\vec{k}\,\hat{U}^{LS}(\vec{k}',\vec{k}) , \tag{A1}$$

and note that, from the defining Eqs. (2.34) and (2.35), the quantities $\hat{U}^{c}(\vec{k}',\vec{k})$ and $\hat{U}^{LS}(\vec{k}',\vec{k})$ are invariant under rotations of the coordinate system and depend on $\cos\theta=\hat{k}'\cdot\hat{k}$ as the only angular variable. Accordingly, we can make the angular momentum expansions (where $a$ stands for either $c$ or $LS$)

$$\hat{U}^{a}(\vec{k}',\vec{k})=4\pi\sum_{JLM}\mathscr{Y}_{JL}^{M}(\hat{k}')\hat{U}_{L}^{a}(k',k)\mathscr{Y}_{JL}^{M\dagger}(\hat{k}) , \tag{A2}$$

$$=4\pi\sum_{LM_L}Y_{L}^{M_L}(\hat{k}')\hat{U}_{L}^{a}(k',k)Y_{L}^{M_L*}(\hat{k}) , \tag{A3}$$

and thus,

$$\hat{U}_{L}^{a}(k',k)=\frac{1}{4\pi}\int d\hat{k}'d\hat{k}\,Y_{L}^{M_L*}(\hat{k}')\hat{U}^{a}(\vec{k}',\vec{k})Y_{L}^{M_L}(\hat{k}) ,$$

$$=\frac{1}{4\pi(2L+1)}\sum_{M_L}\int d\hat{k}'\,d\hat{k}\,Y_{L}^{M_L*}(\hat{k}') \tag{A4}$$

$$\times\hat{U}^{a}(\vec{k}',\vec{k})Y_{L}^{M_L}(\hat{k}) , \tag{A5}$$

$$=\tfrac{1}{2}\int_{-1}^{+1}dx\,P_{L}(x)\hat{U}^{a}(\vec{k}',\vec{k}) , \tag{A6}$$

where $x=\cos\theta=\hat{k}'\cdot\hat{k}$. For the first (central) term of Eq. (A1) the required angular momentum projection $\hat{U}_{LJ}^{c}$ is

thus identified to be $\hat{U}^{c}_{LJ}(k',k)=\hat{U}^{c}_{L}(k',k)$ for both values of $J=L\pm\frac{1}{2}$. The second (complete spin-orbit) term of Eq. (A1) can be treated by writing

$$\frac{i}{2}\vec{\sigma}\cdot\vec{k}'\times\vec{k}\,\hat{U}^{LS}(\vec{k}',\vec{k})=\tfrac{1}{2}\vec{\sigma}\cdot\vec{k}'\hat{U}^{LS}(\vec{k}',\vec{k})\vec{\sigma}\cdot\vec{k}$$
$$-\tfrac{1}{2}\vec{k}'\cdot\vec{k}\hat{U}^{LS}(\vec{k}',\vec{k})\,. \quad \text{(A7)}$$
$$=F(\vec{\sigma},\vec{k}',\vec{k})-G(\vec{k}',\vec{k})\,. \quad \text{(A8)}$$

For the term $F$ we introduce the expansion

$$F(\vec{\sigma},\vec{k}',\vec{k})=4\pi\sum_{JL'LM}\mathscr{Y}^{M}_{JL'}(\hat{k}')F_{JL'L}(k',k)\mathscr{Y}^{M\dagger}_{JL}(\hat{k}) \quad \text{(A9)}$$

which implements conservation of total angular momentum. The components are given by

$$F_{JL'L}(k',k)=\frac{1}{4\pi}\int d\hat{k}'\,d\hat{k}\,\mathscr{Y}^{M\dagger}_{JL'}(\hat{k}')[\tfrac{1}{2}\vec{\sigma}\cdot\vec{k}'\hat{U}^{LS}(\vec{k}',\vec{k})\vec{\sigma}\cdot\vec{k}]\mathscr{Y}^{M}_{JL}(\hat{k})\,. \quad \text{(A10)}$$

When Eq. (A2) is substituted into Eq. (A10), we obtain

$$F_{JL'L}(k',k)=\sum_{J''L''M''}\frac{k'k}{2}\langle JL'M\,|\,\vec{\sigma}\cdot\hat{k}'\,|\,J''L''M''\rangle\hat{U}^{LS}_{L''}(k',k)\langle J''L''M''\,|\,\vec{\sigma}\cdot\hat{k}\,|\,JLM\rangle\,. \quad \text{(A11)}$$

We now make use of the fact that $\vec{\sigma}\cdot\hat{k}$ is a Hermitian, unitary, pseudoscalar operator that commutes with $J^2$ and $J_Z$. It changes the parity but not the norm. This leads immediately to the result

$$\vec{\sigma}\cdot\hat{k}\,\mathscr{Y}^{M}_{JL}(\hat{k})=-\mathscr{Y}^{M}_{J\bar{L}}(\hat{k})\,, \quad \text{(A12)}$$

where $\bar{L}=2J-L$. With this, Eq. (A11) becomes

$$F_{JL'L}(k',k)=\frac{k'k}{2}\sum_{L''}\delta_{L'\bar{L}''}\delta_{L''\bar{L}}\hat{U}^{LS}_{L''}(k',k)\,, \quad \text{(A13)}$$
$$=\delta_{L'L}\frac{k'k}{2}\hat{U}^{LS}_{\bar{L}}(k',k)\,. \quad \text{(A14)}$$

The expected $J$ dependence of this term is implicitly contained in the definition of $\bar{L}$.

The second term of Eq. (A8) is invariant under rotations of the coordinate system and can be expanded as in Eqs. (A2)–(A6). The angular momentum component is $(x=\hat{k}'\cdot\hat{k})$,

$$G_L(k',k)=\tfrac{1}{2}\int_{-1}^{+1}dx\,P_L(x)[\tfrac{1}{2}\vec{k}'\cdot\vec{k}\hat{U}^{LS}(\vec{k}',\vec{k})]\,, \quad \text{(A15)}$$
$$=\frac{k'k}{2}\tfrac{1}{2}\int_{-1}^{+1}x\,dx\,P_L(x)\hat{U}^{LS}(\vec{k}',\vec{k})\,. \quad \text{(A16)}$$

With the help of the recurrence relation

$$xP_L(x)=\frac{1}{2L+1}[(L+1)P_{L+1}(x)+LP_{L-1}(x)]\,, \quad \text{(A17)}$$

Eq. (A16) becomes

$$G_L(k',k)=\frac{k'k}{2}\frac{1}{2L+1}[(L+1)\hat{U}^{LS}_{L+1}(k',k)$$
$$+L\hat{U}^{LS}_{L-1}(k',k)]\,, \quad \text{(A18)}$$

where we have used Eq. (A6) with $a=LS$. The angular momentum expansion of Eq. (A18) for the complete spin-orbit term is thus

$$\frac{i}{2}\vec{\sigma}\cdot\vec{k}'\times\vec{k}\,\hat{U}^{LS}(\vec{k}',\vec{k})$$
$$=4\pi\sum_{JLM}\mathscr{Y}^{M}_{JL}(\hat{k}')\hat{W}^{LS}_{LJ}(k',k)\mathscr{Y}^{M\dagger}_{JL}(\hat{k})\,, \quad \text{(A19)}$$

where

$$\hat{W}^{LS}_{LJ}(k',k)=\frac{k'k}{2}\frac{1}{2L+1}[(2L+1)\hat{U}^{LS}_{\bar{L}}(k',k)$$
$$-(L+1)\hat{U}^{LS}_{L+1}(k',k)$$
$$-L\hat{U}^{LS}_{L-1}(k',k)] \quad \text{(A20)}$$

or equivalently

$$\hat{W}^{LS}_{LJ}(k',k)=C_{LJ}\hat{V}^{LS}_{L}(k',k)\,, \quad \text{(A21)}$$

where

$$\hat{V}^{LS}_{L}(k',k)=-\frac{k'k}{2L+1}[\hat{U}^{LS}_{L-1}(k',k)-\hat{U}^{LS}_{L+1}(k',k)] \quad \text{(A22)}$$

and

$$C_{LJ}=\tfrac{1}{2}[J(J+1)-L(L+1)-\tfrac{3}{4}]\,. \quad \text{(A23)}$$

When this result is combined with the expansion in Eq. (A2) for the central term of the optical potential, we obtain for the total optical potential

$$\hat{U}(\vec{k}',\vec{k})=4\pi\sum_{JLM}\mathscr{Y}^{M}_{JL}(\hat{k}')\hat{U}_{LJ}(k',k)\mathscr{Y}^{M\dagger}_{JL}(\hat{k})\,, \quad \text{(A24)}$$

where the components are

$$\hat{U}_{LJ}(k',k)=\hat{U}^{c}_{L}(k',k)+C_{LJ}\hat{V}^{LS}_{L}(k',k)\,, \quad \text{(A25)}$$

in agreement with the results stated in Eqs. (2.6)–(2.8) of the text.

[1]A. K. Kerman, H. McManus, and R. M. Thaler, Ann. Phys. (N.Y.) **8**, 551 (1959).

[2]L. Ray, *The Interaction Between Medium Energy Nucleons in Nuclei—1982 (Bloomington, Indiana),* Proceedings of the Workshop on the Interaction between Medium Energy Nucleons in Nuclei, AIP Conf. Proc. No. 97, edited by H. O. Meyer (AIP, New York, 1982), p. 121.

[3]A brief preliminary report of some of the material included in this paper has been published as a Rapid Communication: A. Picklesimer, P. C. Tandy, R. M. Thaler, and D. H. Wolfe, Phys. Rev. C **29**, 1582 (1984). In that communication the dashed curves representing the on-shell factorization prescription (OS1) are incorrect beyond $\sim 60°$. The correct behavior of the OS1 curves is discussed in Sec. IV A of the present paper.

[4]W. G. Love and M. A. Franey, Phys. Rev. C **24**, 1083 (1981).

[5]D. H. Wolfe, Ph.D. thesis, Kent State University, 1983 (unpublished).

[6]D. J. Ernst and D. L. Weiss, Phys. Rev. C **26**, 605 (1982); D. J. Ernst, G. A. Miller, and D. L. Weiss, *ibid.* **27**, 2733 (1983).

[7]Y. Alexander and R. H. Landau, Phys. Lett. **84B**, 292 (1979); M. J. Paez and R. H. Landau, Phys. Rev. C **29**, 2267 (1984).

[8]M. Hugi, W. Bauhoff, and H. O. Meyer, Phys. Rev. C **28**, 1 (1983).

[9]J. R. Shepard, J. A. McNeil, and S. J. Wallace, Phys. Rev. Lett. **50**, 1443 (1983); B. C. Clark, S. Hama, R. L. Mercer, L. Ray, and B. D. Serot, *ibid.* **50**, 1644 (1983); M. V. Hynes, A. Picklesimer, P. C. Tandy, and R. M. Thaler, *ibid.* **52**, 978 (1984).

[10]K. M. Watson, Phys. Rev. **89**, 575 (1953).

[11]See, for example, J. M. Irvine, *Nuclear Structure Theory* (Pergamon, Oxford, 1972), and references therein.

[12]A. Picklesimer and R. M. Thaler, Phys. Rev. C **23**, 42 (1981).

[13]G. Takeda and K. M. Watson, Phys. Rev. **97**, 1336 (1955).

[14]A. Picklesimer, Phys. Rev. C **24**, 1400 (1981).

[15]K. M. Maung and P. C. Tandy, Bull. Am. Phys. Soc. **29**, 699 (1984).

[16]C. Möller, K. Dan. Vidensk. Selsk. Mat.-Fys. Medd. **23**, 1 (1945).

[17]L. Wolfenstein, Annu. Rev. Nucl. Sci. **6**, 43 (1956). The NN amplitudes deduced from data have been compiled by R. A. Arndt, private communication.

[18]S. A. Gurvitz, J.-P. Dedonder, and R. D. Amado, Phys. Rev. C **19**, 142 (1979).

[19]F. Petrovich, H. McManus, V. A. Madsen, and J. Atkinson, Phys. Rev. Lett. **22**, 895 (1969).

[20]L. Ray, G. W. Hoffmann, and R. M. Thaler, Phys. Rev. C **22**, 1454 (1980).

[21]C. M. Vincent and S. C. Phatak, Phys. Rev. C **10**, 391 (1976).

[22]G. W. Hoffmann *et al.*, Phys. Rev. Lett. **47**, 1436 (1981).

[23]C. W. DeJager, M. DeVries, and C. DeVries, At. Data Nucl. Data Tables **14**, 479 (1974).

[24]M. V. Hynes, A. Picklesimer, P. C. Tandy, and R. M. Thaler, Los Alamos National Laboratory Report No. LA-UR-84-3151, submitted to Phys. Rev. C.

[25]L. G. Arnold, B. C. Clark, R. L. Mercer, and P. Schwandt, Phys. Rev. C **23**, 1949 (1981).

[26]J. Kelley *et al.*, Phys. Rev. Lett. **45**, 2012 (1980).

[27]B. C. Clark, S. Hama, R. L. Mercer, L. Ray, G. W. Hoffman, and B. D. Serot, Phys. Rev. C **28**, 1421 (1983).

[28]B. A. Brown, Michigan State Shell Model Code, private communication.

[29]B. B. P. Sinha *et al.*, Phys. Rev. C **7**, 1930 (1973); I. Sick and J. S. McCarthy, Nucl. Phys. **A150**, 631 (1970).

[30]A. Picklesimer, E. F. Redish, K. Stricker-Bauer, and P. C. Tandy (unpublished).

[31]A. Rahbar *et al.*, Phys. Rev. Lett. **47**, 1181 (1981).

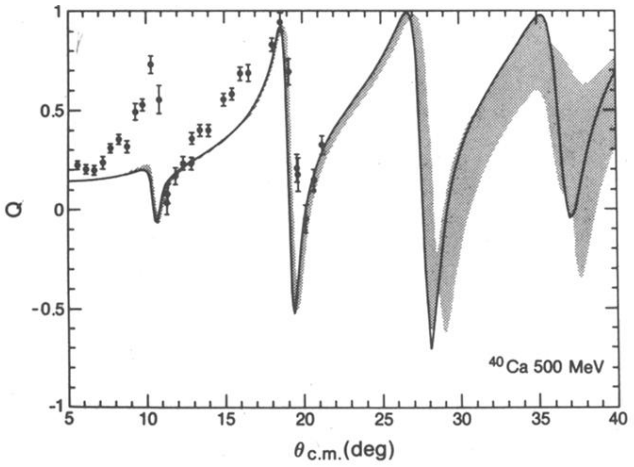


FIG. 10. Spin rotation function $Q$ for $^{40}$Ca at 500 MeV, otherwise as in Fig. 9. The data are from Ref. 31.

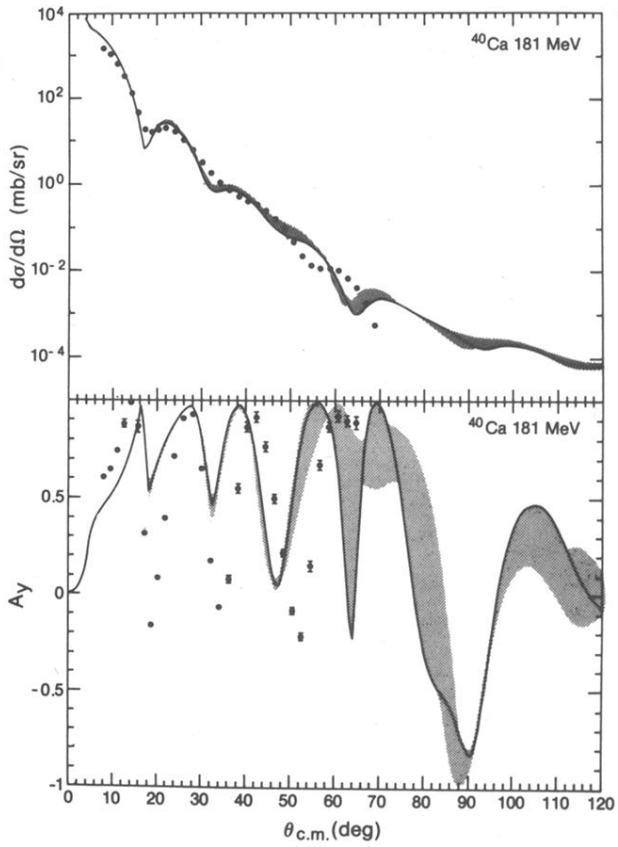


FIG. 11. Same as Fig. 9 except for $^{40}$Ca at 181 MeV. The data are from Ref. 25.

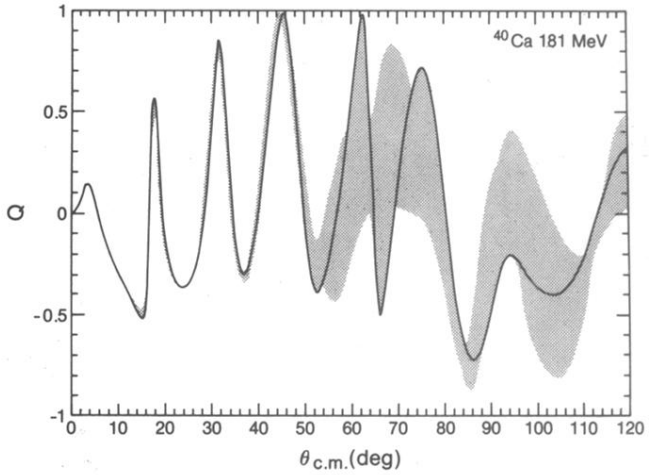


FIG. 12. Same as Fig. 10 except for $^{40}$Ca at 181 MeV.

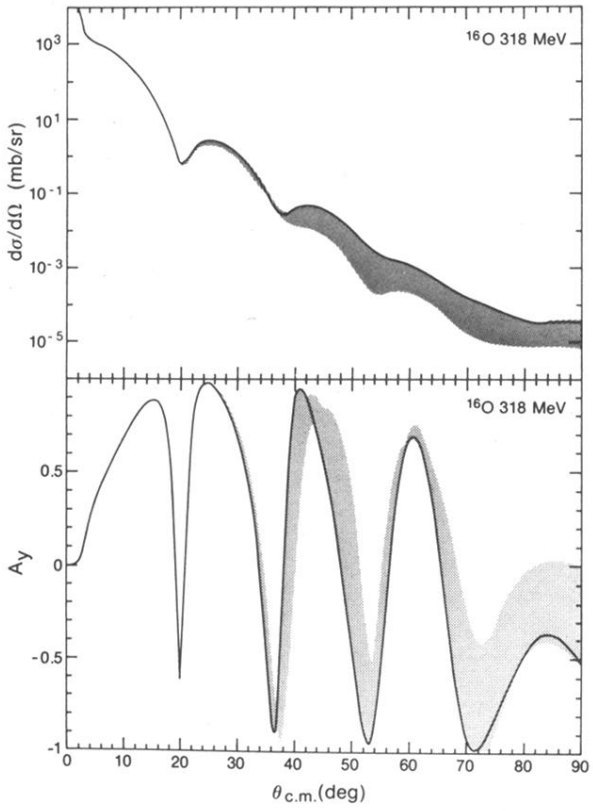


FIG. 13. Same as Fig. 9 except for $^{16}$O at 318 MeV.

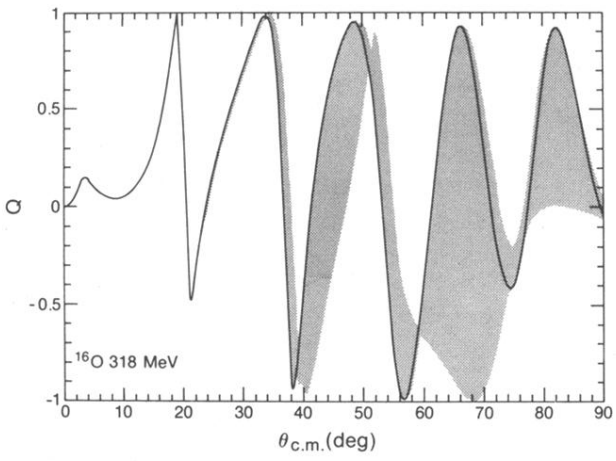


FIG. 14. Same as Fig. 10 except for $^{16}$O at 318 MeV.

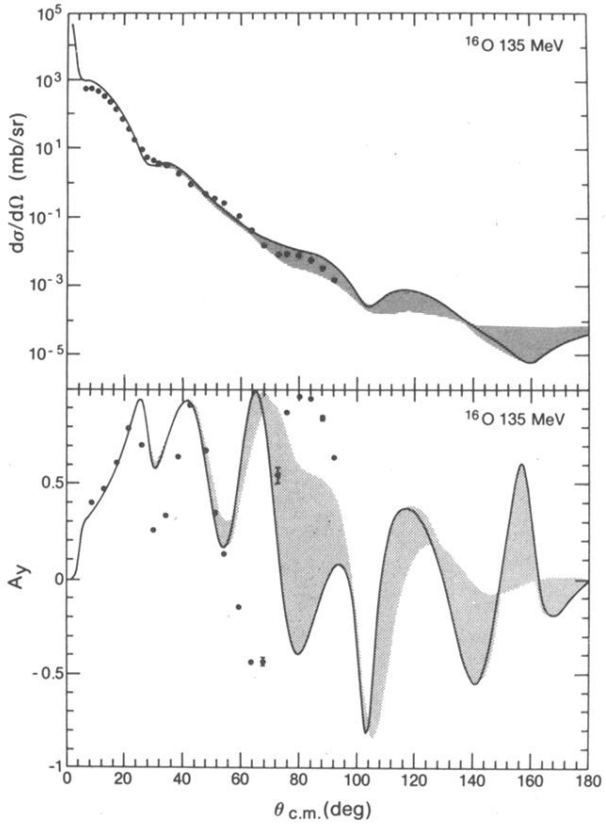


FIG. 15. Same as Fig. 9 except for $^{16}$O at 135 MeV. The data are from Ref. 26.

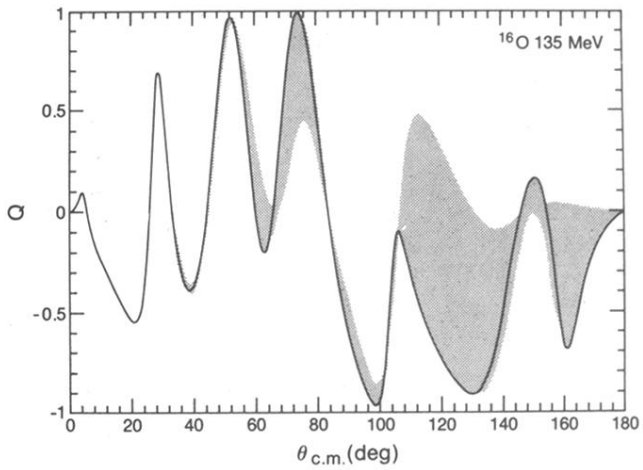


FIG. 16. Same as Fig. 10 except for $^{16}$O at 135 MeV.

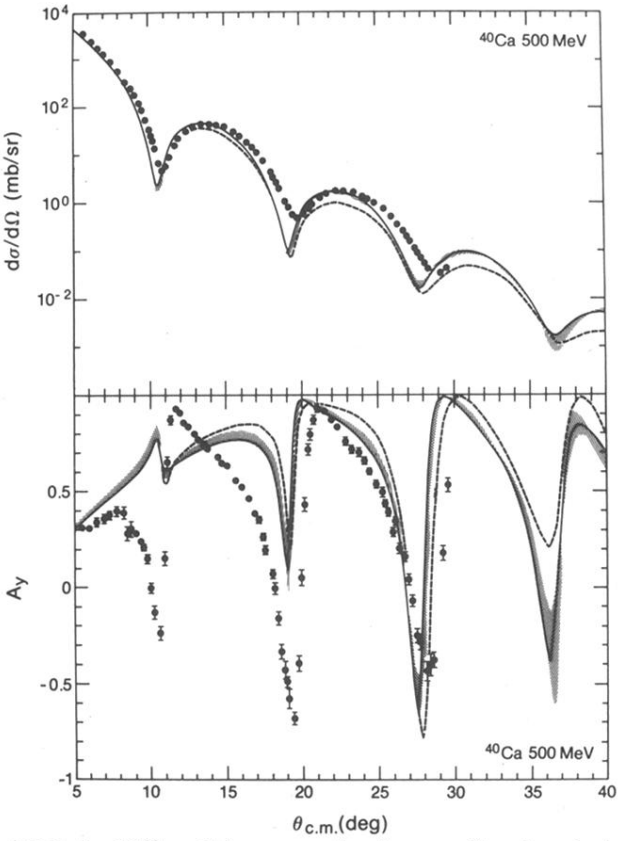


FIG. 2. Differential cross section (top panel) and analyzing power (bottom panel) for protons scattered from $^{40}$Ca at 500 MeV, calculated with the first-order (KMT) optical potential. The solid curve represents the optimum factorization calculation which incorporates off-shell and nonlocal effects, the dashed curve represents the usual on-shell factorization procedure. The shaded band displays an estimate of the range of uncertainties to be expected from approximate treatments of the folding integral. The data are from Ref. 22.

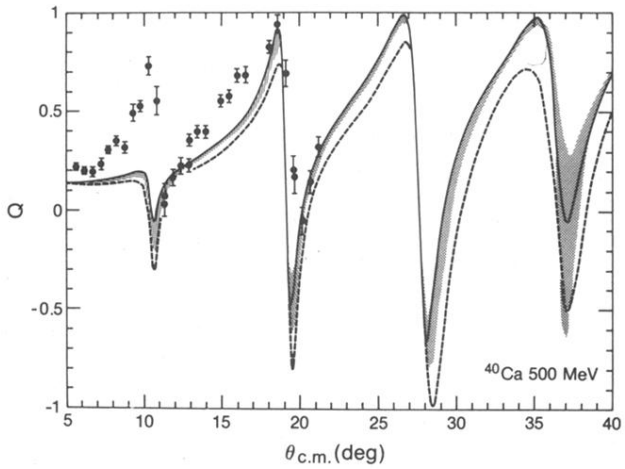


FIG. 3. The spin rotation function $Q$ for protons scattered from $^{40}$Ca at 500 MeV with everything else as in Fig. 2. The data are from Ref. 31.

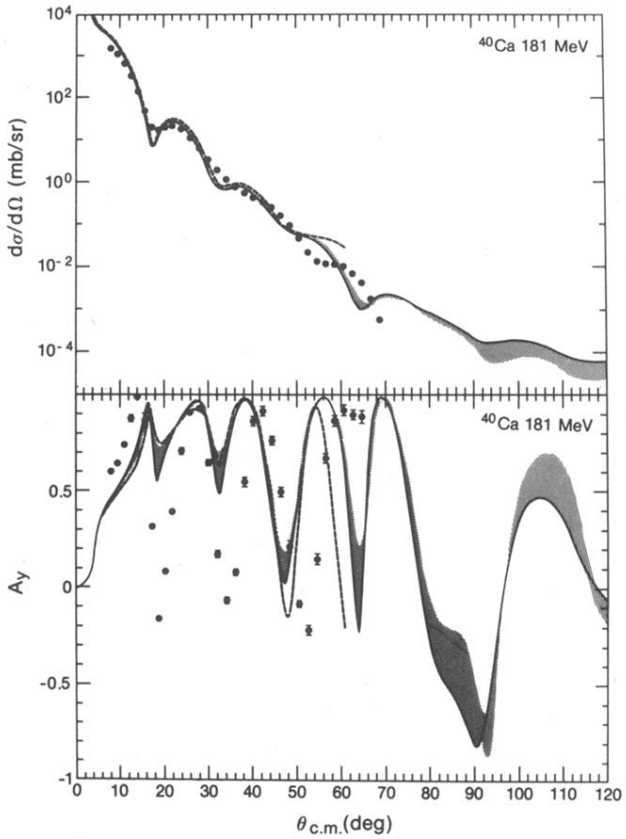


FIG. 4. Same as Fig. 2 except that the proton energy is 181 MeV and the data are from Ref. 25.

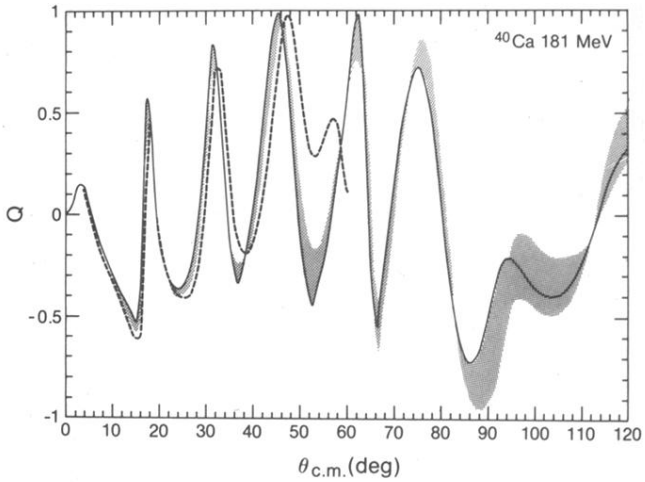


FIG. 5. Same as Fig. 3 except that the proton energy is 181 MeV.

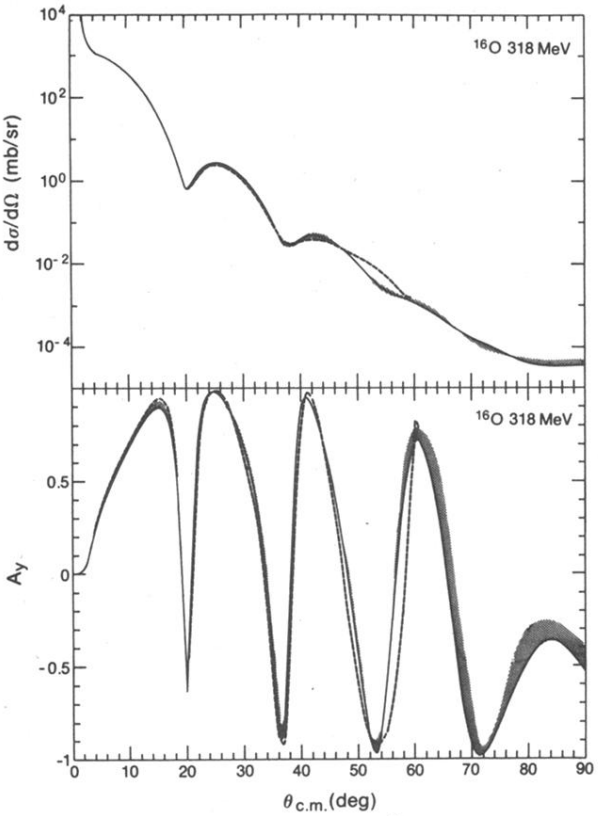


FIG. 6. Same as Fig. 2 except for $^{16}$O at 318 MeV.

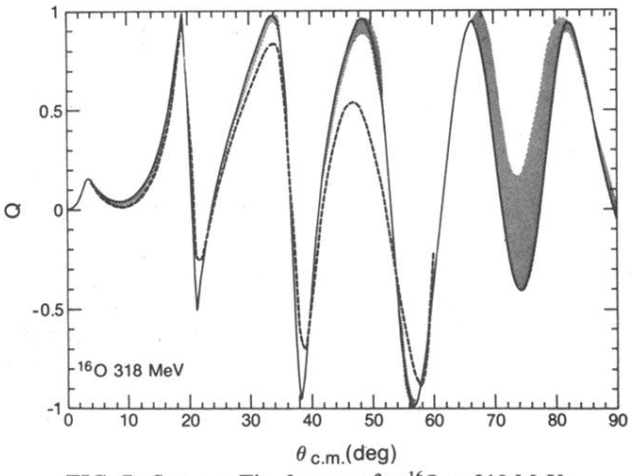


FIG. 7. Same as Fig. 3 except for $^{16}$O at 318 MeV.

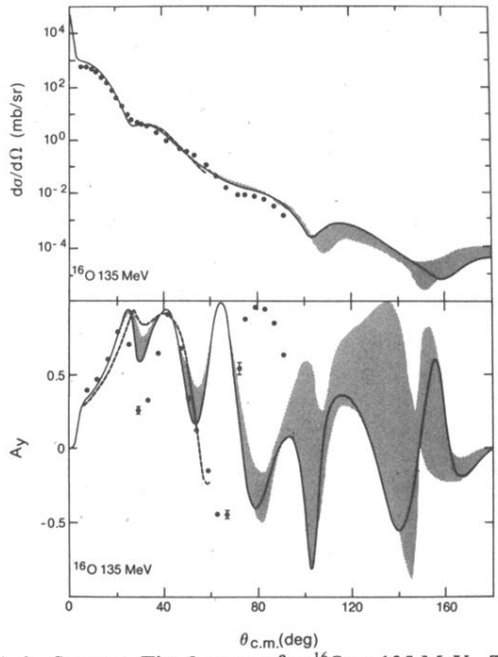


FIG. 8. Same as Fig. 2 except for $^{16}$O at 135 MeV. The data are from Ref. 26.

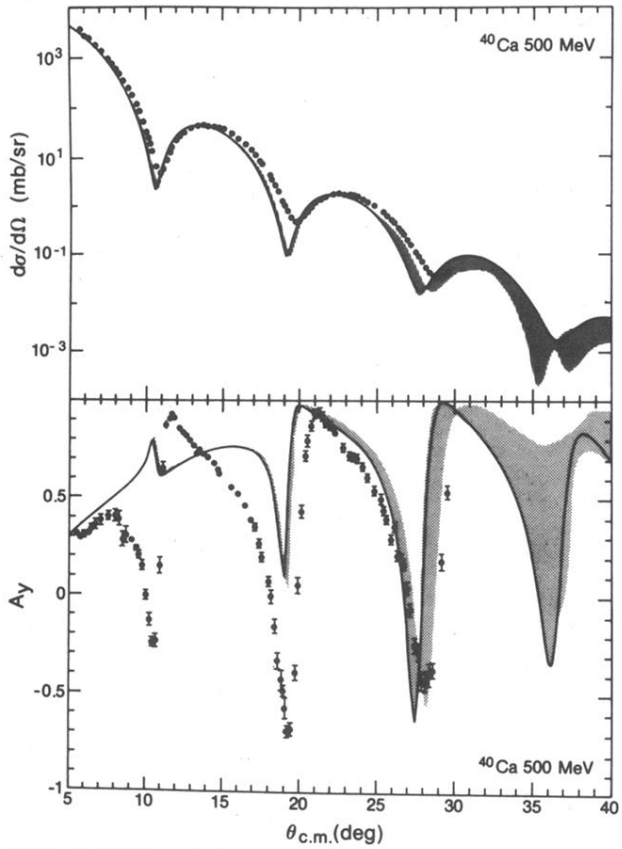


FIG. 9. Differential cross section (top panel) and analyzing power (bottom panel) for protons scattered from $^{40}$Ca at 500 MeV, calculated with the optimum factorization prescription. The shaded band represents the uncertainty in the physical observable due to the uncertainty in the nuclear density. The data are from Ref. 22.